Journal of Rock Mechanics and Geotechnical Engineering 10 (2018) 992–1008

Contents lists available at ScienceDirect

Journal of Rock Mechanics and Geotechnical Engineering

journal homepage: www.rockgeotech.org

Review

Thermo-hydro-mechanical behavior of clay rock for deep geological disposal of high-level radioactive waste

Chun-Liang Zhang

Gesellschaft für Anlagen- und Reaktorsicherheit (GRS), Repository Safety Research Division, Theodor-Heuss-Str. 4, Braunschweig, 38122, Germany

ARTICLE INFO

Article history:
Received 15 November 2017
Received in revised form
26 March 2018
Accepted 27 March 2018
Available online 18 May 2018

Keywords:
Repository
Clay rock
Deformability
Swelling
Self-sealing
Water permeability
Gas migration
Thermal impact

ABSTRACT

In the context of deep geological disposal of radioactive waste in clay formations, the thermo-hydro-mechanical (THM) behavior of the indurated Callovo-Oxfordian and Opalinus clay rocks has been extensively investigated in our laboratory under repository relevant conditions: (1) rock stress covering the range from the lithostatic state to redistributed levels after excavation; (2) variation of the humidity in the openings due to ventilation as well as hydraulic drained and undrained boundary conditions; (3) gas generation from corrosion of metallic components within repositories; and (4) thermal loading from high-level radioactive waste up to the designed maximum temperature of 90 °C and even beyond to 150 °C. Various important aspects concerning the long-term barrier functions of the clay host rocks have been studied: (1) fundamental concept for effective stress in the porous clay-water system; (2) stress-driven deformation and damage as well as resulting permeability changes; (3) moisture influences on mechanical properties; (4) self-sealing of fractures under mechanical load and swelling/slaking of clay minerals upon water uptake; (5) gas migration in fractured and resealed claystones; and (6) thermal impact on the hydro-mechanical behavior and properties. Major findings from the investigations are summarized in this paper.

1. Introduction

Clay rocks are world-widely investigated for deep geological disposal of radioactive waste due to their favorable properties such as large homogeneous rock mass, stable geological structure, extremely low hydraulic conductivity, self-sealing potential of fractures, and high sorption capacity for retardation of radionuclides. Several countries have proposed disposal concepts on the basis of a multi-barrier-system, which comprises the natural geological formations and engineered barriers. In France and Switzerland, for instance, the potential repositories for the disposal of high-level radioactive waste (HLW) will be constructed in the indurated Callovo-Oxfordian (COX) and Opalinus (OPA) argillaceous formations, respectively (Nagra, 2002, 2010, 2014; Andra, 2005, 2015).

In the French concept (Andra, 2005, 2015), the repository will be constructed in the COX clay formation at a depth of about 500 m below the ground surface. HLW canisters will be disposed in horizontal boreholes of 70 cm diameter and tens of meters in length. The boreholes are steel-lined to support the surrounding rock and to ensure emplacement and potential retrieval of waste packages. Each disposal borehole is sealed with swelling clay. The thermal load from HLW is designed to be limited below 90 °C in the rock mass.

In the Swiss concept (Nagra, 2002, 2010, 2014), the repository will be constructed in the OPA formation at a depth of 400–700 m below the ground surface. The facility will include a series of dead-end emplacement tunnels for HLW disposal, which will be excavated in diameter of 2.5–3 m and lengths of several hundred meters. HLW canisters will be emplaced in the middle of the tunnel section and the rest space will be backfilled with expansive bentonite to retard radionuclide migration. The temperature will increase up to 140 °C–160 °C in the buffer on the canister surface and 75 °C–95 °C at the buffer/rock interface.

Construction and operation of a repository will inevitably disturb the rock mass, particularly in the near-field, yielding

E-mail address: chun-liang.zhang@grs.de.

Peer review under responsibility of Institute of Rock and Soil Mechanics, Chinese Academy of Sciences.

https://doi.org/10.1016/j.jrmge.2018.03.006

complex transient thermo-hydro-mechanical (THM) processes and interactions in the natural and engineered barriers for long periods of time of thousands of years. The following disturbances are crucial for the repository safety:

(1) Excavation results in a concentration of the rock stress and redistribution of the pore water pressure, which usually generates an excavation damaged zone (EDZ) around the openings that may act as potential pathways for fluid flow and radionuclide migration into the biosphere.
(2) Support of the openings restricts extension of the EDZ and ensures the operation safety; however, the support efficiency tends to decrease with time due to alternation and damage of the support materials (e.g. steel and concrete) in chemical interactions with pore water solutions.
(3) Ventilation with relatively dry air induces suction and causes release of some pore water out of the rock, which may lead to shrinkage of the pore space and increase the inherent cohesion and friction resistance between particles and hence the strength.
(4) Backfilling and sealing of the repository with suitable materials limit access of groundwater to the waste and thus release of radionuclides via drifts and shafts on one hand, and support the EDZ and limit new damages in host rock on the other hand.
(5) Heat transfer from HLW produces high temperatures in the near-field, which affects the rock stress and deformation, pore water pressure and transport, chemical interactions between pore water, solutes and mineral surfaces, and causes some changes of the barrier properties of the host rock.
(6) Gas generation from corrosion of metallic components may cause gas overpressure if the gas generation rate exceeds the gas dissipation rate in the geological and engineered barrier system, which in turn may generate cracks or dilatational pathways for transport of contaminated water and radionuclides to the aquifer and the biosphere.

Assessment of the long-term performance of a clay host rock and thus the safety of the repository needs comprehensive knowledge of its THM properties and responses to the dynamic conditions (Yu et al., 2014; Bernier et al., 2017; Jobmann et al., 2017). During the last two decades, the THM behavior of the clay rocks has been extensively investigated in the underground research laboratories (URLs) in the COX clay rock at Meuse/Haute-Marne in France (MHM-URL) (Armand et al., 2017) and in the OPA at Mont-Terri in Switzerland (MT-URL) (Bossart et al., 2017). A number of large/full-scale experiments have been conducted in the URLs under realistic repository conditions. The in situ experiments are supported by laboratory tests on samples for providing robust database and for understanding the material behavior. On the basis of the test data, constitutive models and computing codes have been developed for prediction of coupled THM processes in the geological and engineered barriers. From the research activities, comprehensive results have been achieved and published mostly in the Proceedings of the International Conferences on Clays in Natural and Engineered Barriers for Radioactive Waste Confinement (Reims 2002; Tours 2005; Lille 2007; Nantes 2010; Montpellier 2012; Brussels 2015; and Davos 2017). Some of the publications dealing with the THM behavior of clay rocks are listed as follows: Noynaert (2000), Zhang et al. (2007, 2010a, 2013), Bock et al. (2010), Tsang et al. (2012), Li (2013), Menaceur et al. (2015, 2016a), Armand et al. (2017), Bossart et al. (2017), Chen et al. (2017) and Marschall et al. (2017).

Within the framework of the German site-independent research and development program, GRS (Gesellschaft für Anlagen-und Reaktorsicherheit) has participated in the international research projects in the URLs and investigated the THM behavior of both COX and OPA claystones with various important aspects concerning the barrier functions of the clay host rocks, including:

- Conceptual stress model for clay rock;
- Stress-driven deformation, damage, reconsolidation and permeability changes;
- Moisture influences on the mechanical properties and behaviors;
- Self-sealing of fractures;
- Gas migration in fractured and resealed claystones; and
- Thermal effects on the hydro-mechanical behaviors and properties.

This paper presents the most important findings from our investigations. Details can be found in the respective references.

2. A conceptual stress model

The studied clay rocks are a complex material in terms of mineralogical composition, microstructural organization and state of pore water (Yven et al., 2007; Mazurek et al., 2008; NEA Clay Club, 2011; Robinet et al., 2015; Menaceur et al., 2016b). Fig. 1 illustrates schematically the microstructure and the state of pore water in the COX claystone, which is similar for the OPA claystone. The pore sizes in claystones mainly range from nanoscale (<2 nm) in between the parallel platelets of the clay particles to micro- and meso-scale (2–50 nm) between solid particles. The claystones have a clayey matrix embedding other mineral particles (quartz, calcite, and others). The clayey matrix consists of clay particles with strongly adsorbed interlayer water within the sheet structures and with strongly to weakly adsorbed water at the external surfaces. Large pores are filled with water that can freely migrate.

Taking into account the microstructure and the state of pore water, effective stress in claystone has been examined by Horseman et al. (1996), Rodwell et al. (1999) and Zhang (2017a). It is recognized that the effective stress in a water-saturated claystone is partly or even fully transferred by the bound pore water within the interlayer pores and narrow interparticle pores between clay particles. A conceptual stress model was derived by Zhang (2017a), which suggested that the effective stress in a dense clay-water system is transferred through both the solid-solid contact between non-clay mineral grains and the bound water in narrow pores between clay particles. In the model, clay particles including interlayer water are taken as microstructural units since the water molecules in the interlayer are strongly adsorbed and immobile under usually encountered pressure gradients. Fig. 2 shows schematically the stress components acting in any wavy surface that passes through the contact areas between particles in a water-saturated claystone.

The total stress acting on the medium σ_t can be expressed as

$$\sigma_t = \sigma_s + \sigma_l + p_w \quad (1)$$

where σ_s is the contact stress between solid particles, σ_l is the average disjoining (swelling) pressure acting in the bound water between clay particles, and p_w is the pressure acting in free water in macropores. Thus the interparticle or effective stress σ_{eff} consists of two parts acting at solid-solid contact area and in interparticle bound water, i.e.

$$\sigma_{eff} = \sigma_t - p_w = \sigma_s + \sigma_l \quad (2)$$

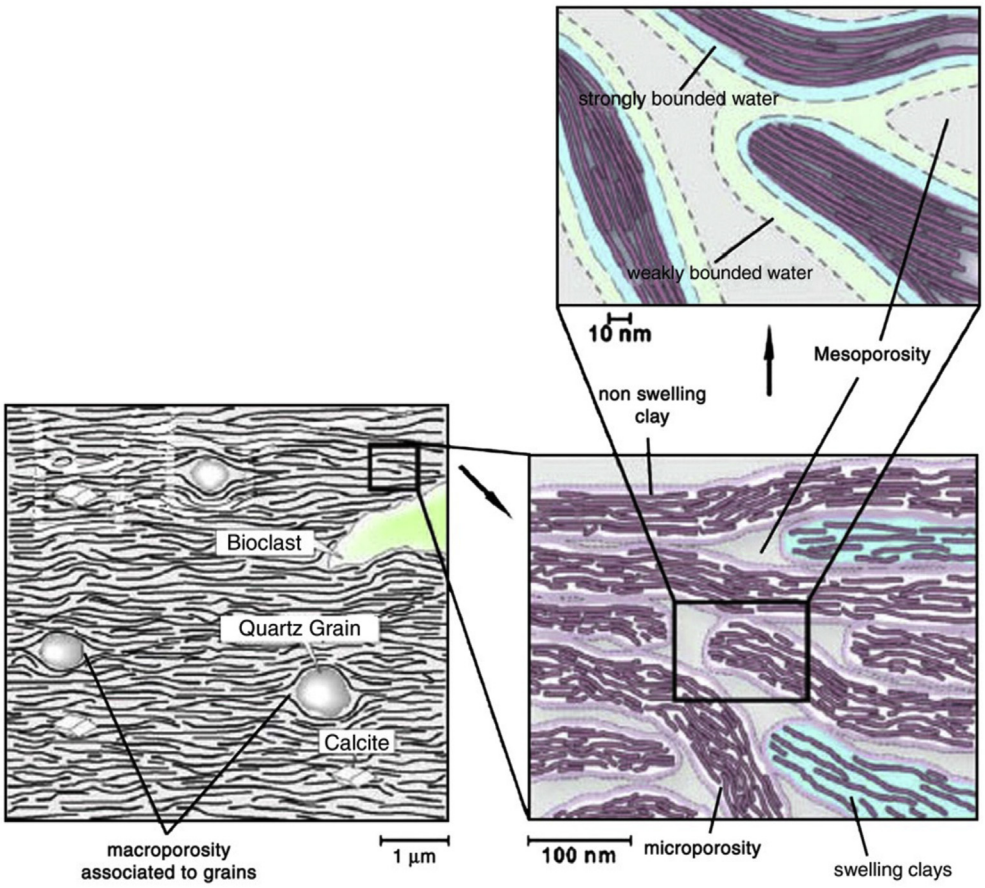

Fig. 1. Schematic sketch of microstructures of the COX claystone (after Yven et al., 2007).

In clay-rich and less cemented materials, the effect of solid-solid contacts between non-clay particles disappears, i.e. $\sigma_s \to 0$, so that the effective stress is mostly carried by the bound pore water and is equivalent to the swelling pressure, i.e. $\sigma_{eff} \Leftrightarrow \sigma_l$. Conversely, if a claystone contains a large number of non-clay particles and/or is strongly cemented, the effect of bound water is negligible, i.e. $\sigma_l \to 0$, and thus the externally applied load will be transferred through the solid-solid grain contacts, i.e. $\sigma_{eff} \Leftrightarrow \sigma_s$. This concept provides a reasonable view to the nature of the effective stress in clay rock and clay soil, forming the fundamental basis for understanding their THM behavior. This stress concept has been already confirmed by experimental evidence (Zhang et al., 2013; Zhang, 2017a) (see Section 4.1).

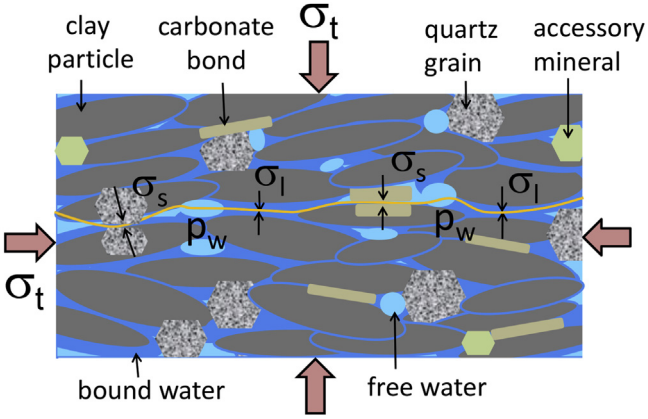

Fig. 2. Conceptual stress model for water-saturated claystone.

3. Deformation and damage

3.1. Characterization of samples

Most of the mechanical tests were carried out on COX samples that were extracted from boreholes drilled horizontally parallel to bedding planes at the −490 m main level of MHM-URL. In order to prevent desaturation and damage, the drilled cores were confined in special cells developed by Andra (Conil et al., 2018) and stored in a climate-controlled room at 22 °C. Cylindrical samples were carefully prepared from the cores.

The COX claystone at the sampling locations contains 27%–42% clay minerals, 28%–38% carbonates, 26%–36% quartz and small amounts of other minerals (Andra, 2005). The physical properties of the samples were determined: grain density $\rho_s = 2.7 \pm 0.01$ g/cm^3, bulk density $\rho_b = 2.4 \pm 0.02$ g/cm^3, porosity $\phi = 16.8\% \pm 1\%$, water content $w = 6.5\% \pm 0.8\%$, and degree of water saturation $S_l = 90\% \pm 6\%$. In order to minimize the effects of sampling-induced microfissures and desaturation, the samples before testing were pre-consolidated by hydrostatic compression up to the in situ rock stress and even higher stresses.

3.2. Short-term behavior

The short-term mechanical behaviors of the clay rocks were examined on the pre-consolidated samples in triaxial compression

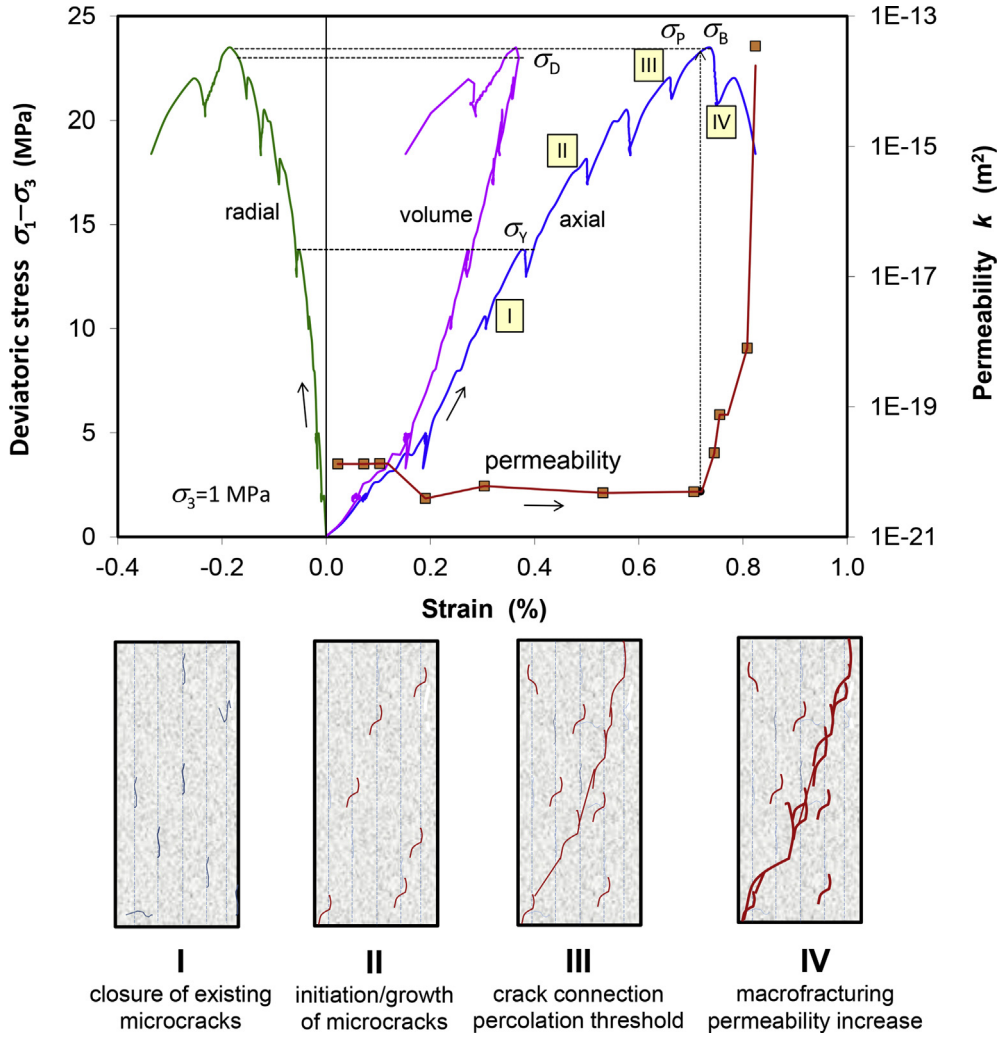

Fig. 3. Stress-strain-permeability behavior of COX claystone including stress thresholds of yield σ_Y, dilatancy σ_D, percolation σ_P, and failure σ_B.

tests by measurements of deformation and gas permeability (Zhang and Rothfuchs, 2004, 2008; Zhang, 2015a, 2016a). Deviatoric loading was performed by axial compression at a rate of 10^{-6} s^{-1} and at a lateral confining stress of 0–12 MPa. Fig. 3 shows the typical strain and permeability responses of the COX claystone to deviatoric loading with some stress relaxation phases for the measurement of gas permeability.

The stress-strain-permeability behavior can be characterized in four sequential stages:

(I) The stress–strain curves start with linear axial compression ε_1, radial extension ε_3 and volumetric compaction ε_v until a deviation appears at a deviatoric stress σ_Y, named yield stress.

(II) This yield point indicates a certain damage of the inner pore structure leading to plastic volumetric compaction. With increasing deviatoric stress, the microcracks are created and grow so that the volumetric compaction changes over to dilatation. The corresponding deviatoric stress σ_D is referred to as dilatancy or damage threshold.

(III) Exceeding the dilatancy threshold, the microcracks grow and propagate much faster with further deviatoric loading. When some of the microcracks coalesce to a continuous fracture, the permeability increases spontaneously. The corresponding deviatoric stress σ_P is called percolation threshold. The rapid development of fractures after the dilatancy threshold leads to failure at a peak stress σ_B. Fracture percolation and peak failure occur almost simultaneously, i.e. $\sigma_P \approx \sigma_B$.

(IV) Beyond this peak point, the permeability k increases by several orders of magnitude accompanied by only little additional crack opening or dilatancy. This implies that the rapid permeability rise is governed by the increasing connectivity of the stress-induced cracks.

The damage and the resulting permeability change are inhibited by increasing the lateral confining stress. As the lateral stress is increased, the inner structure of the claystone becomes more compacted, increasing the strength. Fig. 4 shows the critical stresses at yield σ_Y, dilatancy σ_D, percolation σ_P and peak failure σ_B, as function of the lateral stress σ_3.

The relation of the peak strength σ_B to the minor principal stress σ_3 can be approached by Hoek-Brown criterion:

$$\sigma_B = \sigma_{1B} - \sigma_3 = \left(m\sigma_c\sigma_3 + s\sigma_c^2\right)^{1/2} \quad (3)$$

where σ_c is the uniaxial compressive strength which is determined to be $\sigma_c = 19$ MPa, and the other parameters $m = 4$ and $s = 1$ for the

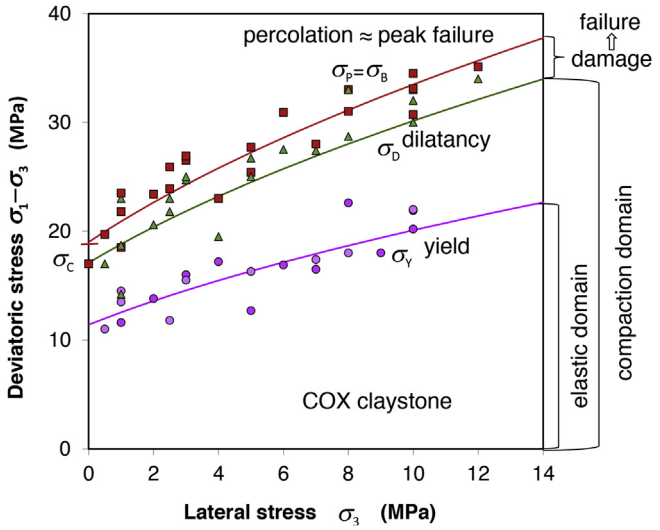

Fig. 4. Stress boundaries of yield, dilatancy, percolation and peak failure for COX claystone.

COX claystone. It is observed that the dilatancy boundary σ_D is about 93% of the failure envelope. As mentioned above, high stresses above the dilatancy boundary drive the development of microcracks to coalescence and thus to rupture.

Based on the permeability evolution observed during loading at different confining stresses (Fig. 5), a percolation model was proposed by Zhang (2016a) for the fracturing-induced permeability, which is assumed to be contributed by the connectivity and the conductivity of cracks, and can be expressed by

$$k = k_f P = k_o \exp(-\gamma\sigma_3)\left[1-\exp\left(-\frac{\Delta\varepsilon_D}{\varepsilon_P}\right)\right] \quad (4)$$

where k_f is the ultimate permeability of the fractured rock with fully interconnected cracks and P is the percolation probability defining the fraction of cracks belonging to the conductive part of a network. The ultimate fracture permeability k_f decreases with increasing minor principal stress σ_3 following an exponential function: $k_f = k_o \exp(-\gamma\sigma_3)$, where k_o is the permeability at $\sigma_3 = 0$ and γ is a parameter characterizing the dilatability of the interconnected cracks. The percolation probability P is expressed as an exponential function of volumetric dilatancy: $P = 1 - \exp(-\Delta\varepsilon_D/\varepsilon_P)$, where $\Delta\varepsilon_D = |\varepsilon_v - \varepsilon_P|$ is the dilatancy after the percolation threshold at ε_P.

Using the estimated values of the parameters, $k_o = 3 \times 10^{-13}$ m^2 and $\gamma = 1.9$ MPa^{-1}, the permeability variations observed after exceeding dilatancy ($\Delta\varepsilon_D \geq 0$) under different lateral stresses are predicted by the model as shown in Fig. 5. It is evident that the permeability evolution with the spontaneous increase due to the formation of a continuous crack network ($\Delta\varepsilon_D = 0 \rightarrow 0.05\%$) and with the subsequent slowdown due to further development of the network ($\Delta\varepsilon_D > 0.05\%$) can be reasonably revealed by the model.

3.3. Long-term behavior

The long-term performance of a repository is strongly dependent on the long-term deformability of the host rock. This important issue was investigated on the COX and OPA claystones with natural water contents in triaxial creep experiments. Fig. 6 presents the results obtained on water-saturated COX and OPA samples subjected to the low deviatoric stresses of $\Delta\sigma = \sigma_1 - \sigma_3 = 0.8$–3.5 MPa parallel to bedding planes. It is obvious that the axial and

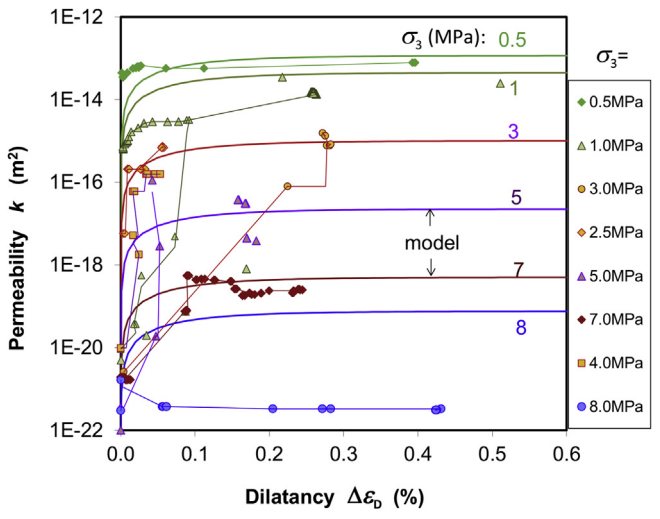

Fig. 5. Prediction of the fracturing-induced permeability in the claystone using the percolation model.

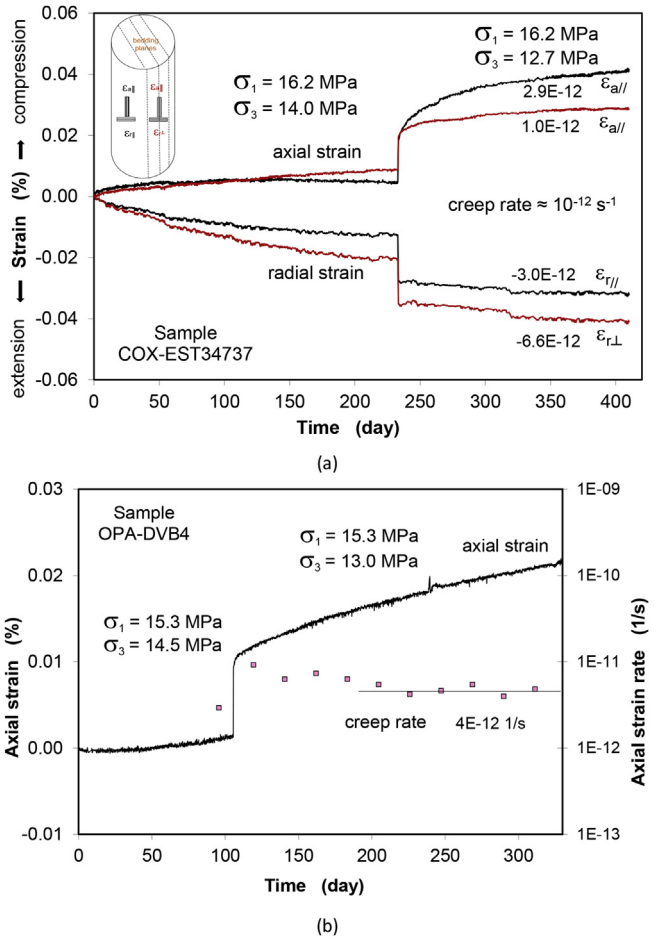

Fig. 6. Creep of water-saturated (a) COX and (b) OPA claystones under low deviatoric stresses of 0.8–3.5 MPa.

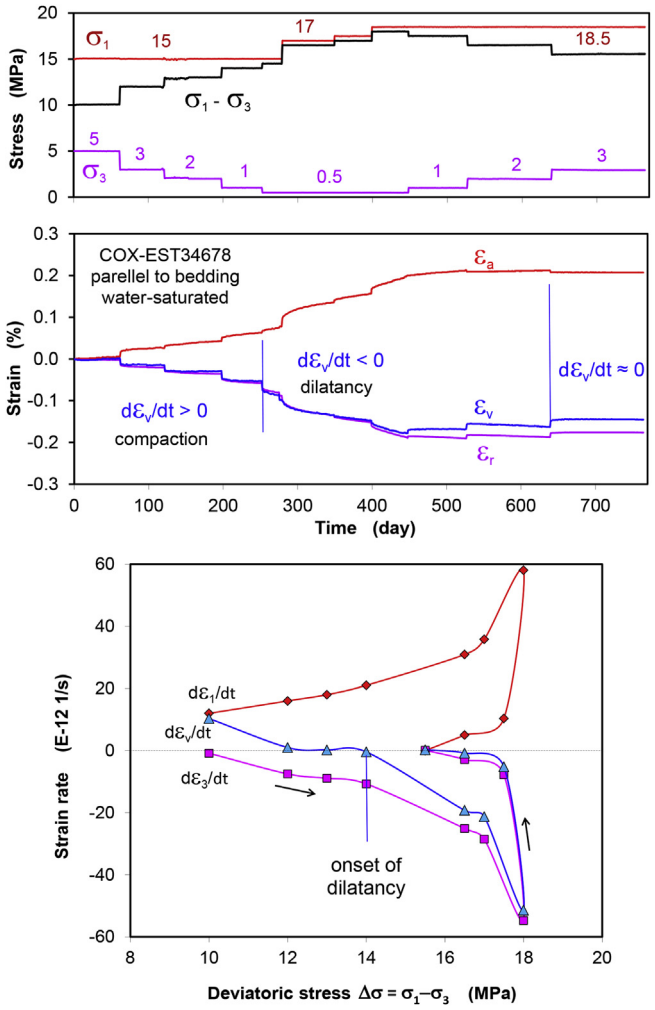

Fig. 7. Creep of COX claystone under multistep triaxial stresses.

radial strains locally measured by means of strain gages increase gradually with time at each load step. The strain rates decrease during the first transient phase within two to three months and approach asymptotically quasi-constant values. The quasi-stationary creep rates are very low, at around 10^{-12} s^{-1}. The extremely low stresses at which creep occurs suggest that there exists practically no stress threshold for onset of creep in the saturated claystones.

Fig. 7 shows another creep test on COX claystone under multi-step triaxial loads over two years. During the first phase at an axial stress $\sigma_1 = 15$ MPa, the lateral stress σ_3 was stepwise reduced. At $\Delta\sigma = \sigma_1 - \sigma_3 < 14.5$ MPa, the volumetric strain rate was still positive, i.e. $d\varepsilon_v/dt > 0$, indicating a compaction process and thus no damage. The quasi-stationary creep rate increased almost linearly with increasing stress. At $\Delta\sigma = 14.5$ MPa, the volumetric strain rate became negative, i.e. $d\varepsilon_v/dt < 0$, suggesting onset of dilatancy or damage. Thus, creep was accelerated by further damaging at the subsequently increased stresses that reached up to $\Delta\sigma = 18$ MPa. When the deviatoric stress was stepwise decreased by increasing σ_3 to 3 MPa, the creep with damage evolution was impeded. The difference in creep rate at a stress reached by uploading and unloading indicates hardening effects.

Mitchell (1976, 1992) has derived a constitutive equation for creep of clay soils through thermodynamic analysis of soil flow by

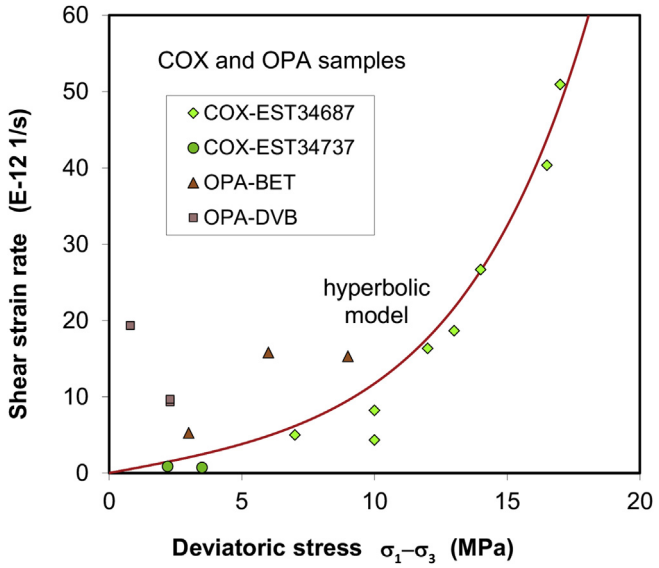

Fig. 8. Stationary shear creep rates of water-saturated COX and OPA claystones as function of deviatoric stress.

application of the absolute reaction-rate theory. This model has been slightly modified and applied by Zhang et al. (2013) and Zhang (2015a) for mathematical description of the stationary creep of clay rocks in terms of the stationary shear creep rate in relation to the deviatoric stress and temperature:

$$\dot{\varepsilon} = A \exp\left(-\frac{Q}{RT}\right) \sinh(\alpha \Delta\sigma) \tag{5}$$

where $\dot{\varepsilon}$ is the stationary shear creep rate (s^{-1}), T is the absolute temperature (K), R is the universal gas constant (8.31433 × 10^{-3} kJ mol^{-1} K^{-1}), Q is the apparent activation energy (kJ mol^{-1}), A is a factor in s^{-1} depending on the inherent properties of the material, and α is a parameter in MPa^{-1}. These parameters were determined from the creep data obtained along uploading path for the COX claystone: $A = 2.1 \times 10^{-4}$ s^{-1}, $\alpha = 0.2$ MPa^{-1} and $Q = 45$ kJ mol^{-1}.

Fig. 8 shows a reasonable agreement of the model with the measured creep rates for the COX claystone. The relatively high creep rates observed on the OPA claystone are probably due to its higher content of clay minerals (~65%) compared to the COX claystone (~40%). At low stresses below about 10 MPa, the time-dependent deformation of water-saturated claystone is likely controlled by diffusive mass transfer or pressure solution processes in interfaces between grains in accordance to Rutter (1983). At high stresses, the creep rate increases exponentially. This may indicate increasing contributions from slips and ruptures of water-films at interparticle contacts between clay particles and solid-solid contacts between non-clay particles. Accumulation of the micro-ruptures between particles results in development of micro-fractures and ultimately in failure (Zhang et al., 2013; Zhang, 2015a). This microstructural hypothesis requests to be validated by microscopic observations.

4. Responses to moisture change

4.1. Stress response to moisture change

Stress response of claystone to moisture change was studied with the so-called uniaxial swelling test method specially

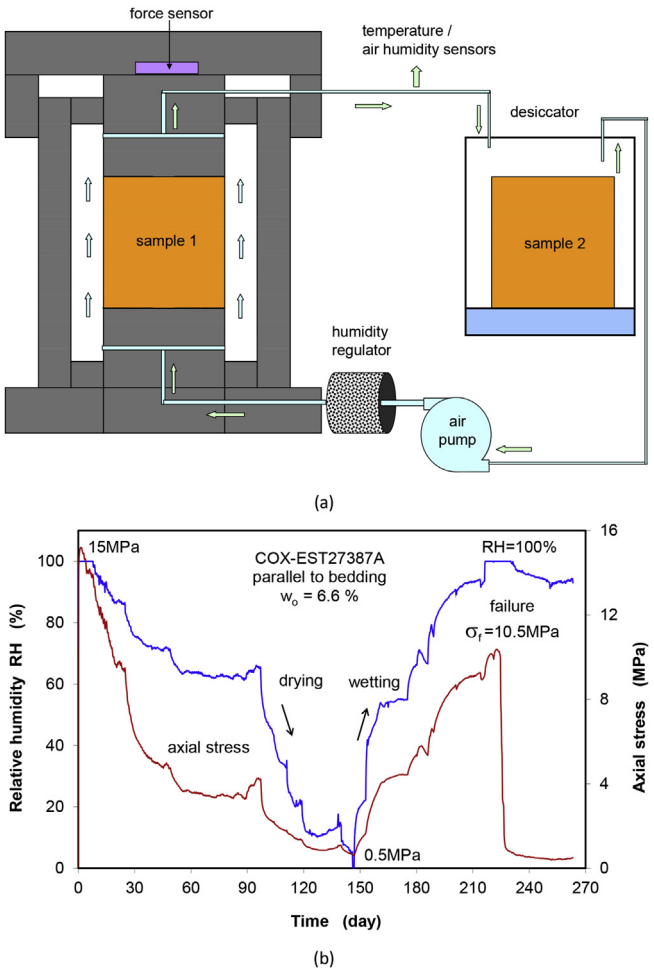

Fig. 9. (a) Principle of uniaxial swelling test under axially-fixed and laterally-unconfined conditions and (b) Stress response to humidity change surrounding a claystone.

developed by our laboratory (Zhang and Rothfuchs, 2007; Zhang et al., 2010b, 2013; Zhang, 2017a; b). A sample is axially loaded to a desired level and then fixed without lateral confinement (Fig. 9a). Under the axially-fixed and laterally free conditions, the sample is dried and wetted by circulating air with varying humidity around the surface, where response of the axial stress is monitored. The resulting variation of water content is measured on an accompanying sample of the same size in the same air circulating system outside the cell.

Fig. 9b shows the typical response of the axial stress to humidity change. It can be seen that drying led to a decrease in the axial stress from the preload of 15 MPa down to nearly zero and then the subsequent wetting caused an increase to a high level of 10.5 MPa where failure occurred due to wetting-induced alteration of the inner structure. This stress value is consistent with the uniaxial strength of the claystone at a high water content of 7.7% reached after a month of wetting in water vapor. Actually, drying causes release of the adsorbed water and conversely wetting lets water molecules enter the pores, being adsorbed on internal and external surfaces of clay particles, forming double layers being compressed in narrow pores and resulting in repulsive forces against the rigid confinement in axial direction. The variation of the stress with drying and wetting implies that the adsorbed water-films are capable of carrying effective stress and thus confirms the stress concept (Eq. (2)) discussed earlier in Section 2. Actually, the axial stress recorded is the effective one (σ_{eff}), since no water pressure was applied to the sample and thus the pressure in the free water in macropores is zero, i.e. $p_w = 0$. The axial effective stress is directly related to the swelling pressure σ_l in the axial direction, i.e. $\Delta\sigma_{eff} = \Delta\sigma_l$. The buildup of the uniaxial swelling pressure without lateral confinement indicates its tensor expression (Horseman et al., 1996; Rodwell et al., 1999), which differs from the isostatic pressure state of free water in macropores.

Obviously, the swelling pressure σ_l is dependent on saturation degree of bound pore water, as shown in Fig. 10 representing the σ_l data in relation to the degree of total water saturation. The saturation degrees of the different types of pore water (interlayer water, interparticle bound water, and free water) are also illustrated schematically.

It can be seen from Fig. 10 that:

(1) The pre-applied axial stress of $\sigma_o = 15$ MPa decreases with desaturation to a minimum value of $\sigma_s = 0.5$ MPa at a residual saturation degree of $S_r = 15\%$, below which no stress changes occur.
(2) The resaturation increases the stress to $\sigma_{ls} = 9.5$ MPa at full saturation ($S_l = 100\%$), and even after that, the stress increase continues with more water uptake to a maximum value of $\sigma_p = 10.5$ MPa, so that the total maximum swelling pressure is the sum of $\sigma_l = \sigma_p - \sigma_s = 10$ MPa.
(3) The stress varies almost linearly with degree of water saturation in a range of $S_r \le S_l < 80\%$ along drying path and $S_r \le S_l < 90\%$ along wetting path.

Based on the test results and taking the fractions of the different contact areas (solid-solid, bound water-films and free pore water) into account, a relationship of the effective stress to the saturation degree of bound pore water was approximately derived by Zhang et al. (2013) and Zhang (2017a):

$$\begin{aligned}\sigma_{eff} &= \sigma_s + \sigma_l = \sigma_s + \pi_D S_e + \pi_O(\Delta w)\\ &= \sigma_s + \pi_D \frac{S_l - S_o - S_r}{1 - S_o - S_r} + \pi_O(\Delta w)\end{aligned} \quad (6)$$

where S_e is the effective saturation degree of bound pore water, S_l is the saturation degree of total pore water, S_o is the saturation degree of free pore water ($S_o = 0$ for the tested claystone), S_r is the residual saturation degree of the remaining water in the interlayer and adsorbed on the external surfaces as the clay particles are disconnected, π_D is the local net disjoining pressure in the bound pore water before full saturation, π_O is the swelling pressure after full saturation upon water uptake Δw, σ_s is the contact stress between solid particles at the residual degree S_r of water saturation, and σ_l is the swelling pressure acting in the bound water between clay particles and consists of two parts by $\pi_D S_e$ before full saturation and $\pi_O(\Delta w)$ after full saturation.

Because the water sorption process in the claystones is not really clear, this preliminary model has to be modified further and needs more precisely physical interpretations. It seems also possible to establish a relation of the effective stress directly to suction, because the saturation degrees of the different types of pore water and the buildup of swelling pressures are governed by suction for a given clay material.

4.2. Swelling upon water uptake

The studied claystones possess adsorption potentials, under which an amount of water can be taken up from the humid

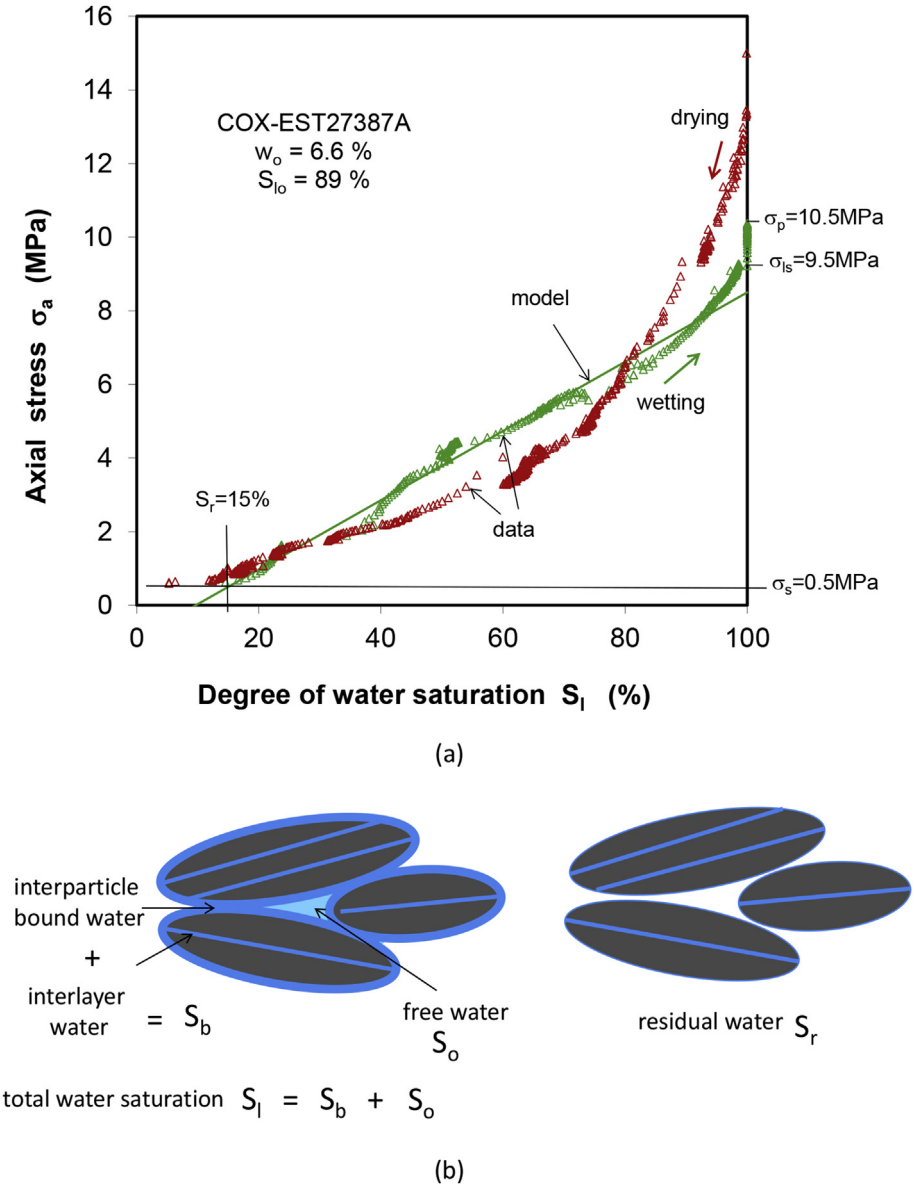

Fig. 10. (a) Effective stress and swelling pressure as a function of degree of water saturation and (b) Schematic of saturation of interlayer, interparticle bound and free water in clay.

environment. The water uptake enlarges the distances between clay particles and between the interlayers in clay minerals, causing macroscopic swelling. The water uptake and the resulting swelling depend on the humid environment and confining conditions.

During the observation of stress response to drying and wetting on the axially-fixed COX sample (cf. Fig. 9), its radial strain was also monitored (Fig. 11a) and in parallel, the variation of water content and deformation in axial and radial directions were measured on the other accompanying sample under unconfined conditions (Fig. 11b). The results from the unconfined sample (Fig. 11b) show that drying caused evaporation and release of bound pore water, resulting in collapse of the pore structure to macroscopic shrinkage. A larger shrinkage was observed in radial direction normal to bedding compared to the axial shrinkage parallel to bedding. Under the axially-fixed condition, the drying-induced reduction of the axial stress (Fig. 9) was accompanied by shrinking in radial direction (Fig. 11a). The subsequent wetting increased the water content to the initial value of 7.2%, resulting in a radial expansion of the axially-fixed sample (Fig. 11a) and expansion of the unconfined sample in all directions (Fig. 11b). However, the free swelling observed on the unconfined sample is anisotropic with larger radial strain normal to bedding compared to the axial strain parallel to bedding. The anisotropic response of the claystones to moisture change was also observed by other research groups (Valès et al., 2004; Wan et al., 2013; Wang et al., 2013; Yang et al., 2013; Minardi et al., 2017).

Under unconfined conditions, the claystones can take up great amounts of water up to 12%–15% in water vapor, much more than that of 7%–8% in the in situ confined conditions. The increase in water content contributes to the volumetric expansion up to 8%–12%, as shown in Fig. 12 comparing the swelling capacities of the COX and OPA claystones by wetting with water vapor at relative humidity (RH) of 100%. The OPA claystone with higher clay content of ~65% takes more water and expands more compared to the COX with clay content of ~40%.

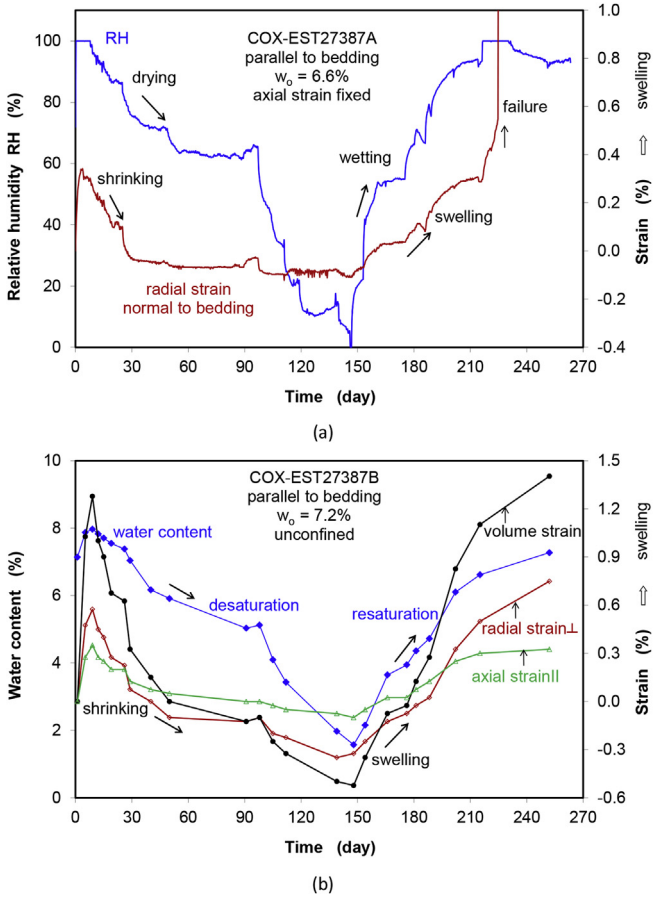

Fig. 11. Strain responses of COX claystone samples under (a) axially-fixed and (b) unconfined conditions to humidity change.

4.3. Influence of water content on strength

Increasing water content results in widening of the distances or thickness of bound water-films between clay particles and in turn degradation of the inherent cohesion and friction resistance. Thus the stiffness and strength are degraded with increasing water content. Conversely, drying causes release of the adsorbed water, leading to more solid-solid contacts between particles, so that the inherent cohesion and friction resistance increase and enhance the stiffness and strength. Fig. 13 shows the results of uniaxial compression tests on the COX claystone with different water contents of w = 1.4%–7.7%. It is obvious that the elastic stiffness, dilatancy and peak failure strengths increase significantly with decreasing water content. The maximum peak strength of about 50 MPa is reached at w = 1.4%, four times higher than that of 10 MPa at w = 7.7%. Similar observations were also made by other research groups on the claystones (Blümling et al., 2007; Zhang et al., 2014; Amann et al., 2017).

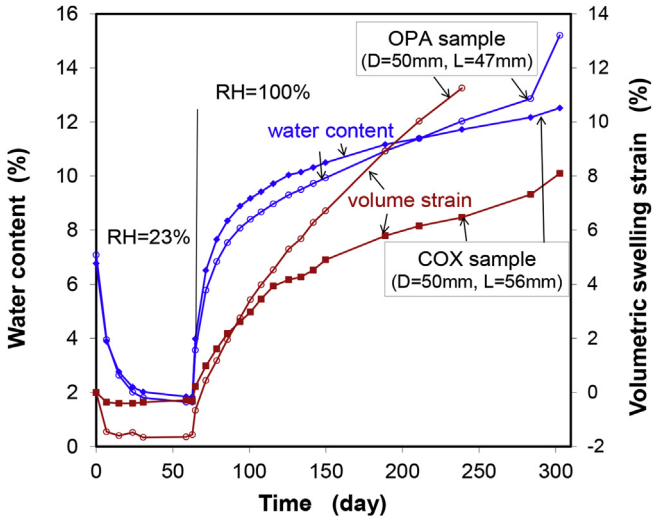

Fig. 12. Free swelling of COX and OPA claystones during wetting with vapor.

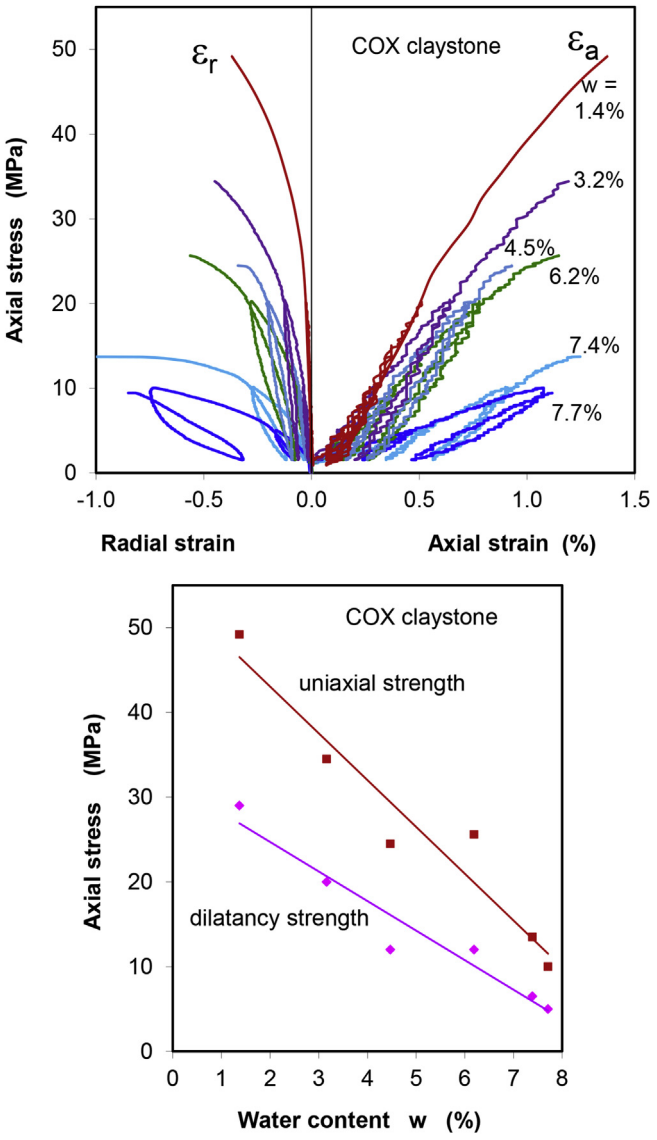

Fig. 13. Influence of water content on the uniaxial stress–strain behavior, dilatancy and failure strength of COX claystone.

5. Sealing of fractures

Because of the rheological deformability and swelling capability of the claystones presented before, a recovery process of the EDZ can be expected due to combined impact of the progressive deformation of the clay host rock, the increasing resistance of the engineered barriers, and the swelling/slaking of clay minerals into

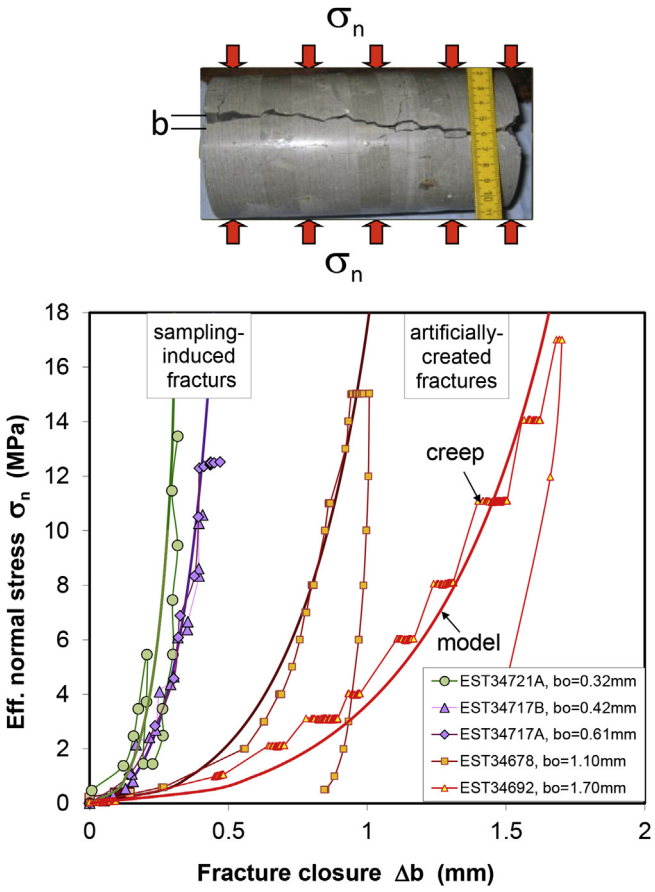

Fig. 14. Fracture closure-normal stress relationship obtained on COX claystone.

fracture interstices during the post-closure phase of the repository. This important issue has been intensively investigated with artificially-cracked samples under various THM conditions (Davy et al., 2007; Zhang and Rothfuchs, 2008; Zhang, 2009, 2011; 2013, 2016a; Bock et al., 2010; Zhang et al., 2010a, 2013; Auvray et al., 2015). Some typical results from our experiments (Zhang, 2009, 2011, 2013) are presented below.

5.1. Under compression

Axially-cracked samples were compressed in triaxial cells, whereby closure of fractures and gas permeability were measured. Fig. 14 illustrates some results of fracture closure (Δb) under normal stresses (σ_n). All the σ_n-Δb curves express the nonlinear behavior, involving the decayed fracture closure and the hysteresis cycle by loading/unloading. Fracture closure evolves faster at large apertures in the initial stage and then closure rates decrease with increase in normal stiffness of the fractures at small apertures. The relationship of fracture closure with effective normal stress can be approximated by an exponential equation:

$$\Delta b = b_o\left[1 - \exp\left(-\alpha\sigma_n^{\xi}\right)\right] \tag{7}$$

where b_o is the initial aperture equivalent to the maximum aperture closure, and α and ξ are the constants. If the stress tends to infinity ($\sigma_n \to +\infty$), the fractures will be fully closed, i.e. $\Delta b \to 0$. Fitting the data derives a unique set of the parameters $\alpha = 0.3$ and $\xi = 0.5$ for the samples with different initial apertures of $b_o = 0.32$–1.7 mm.

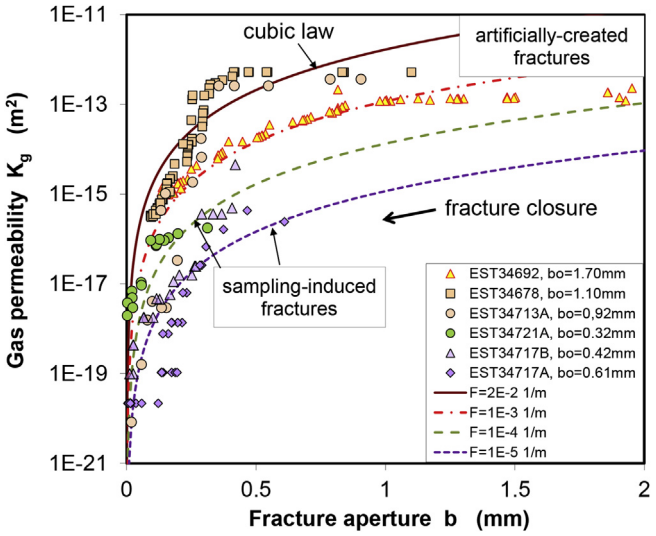

Fig. 15. Fracture permeability–aperture relationship obtained on COX claystone.

The fracture closure results in a decrease in gas permeability from the initial value of 2×10^{-13}–5×10^{-13} m^2 down to 3×10^{-16}–7×10^{-16} m^2 for the large initial apertures ($b_o = 1.1$–1.7 mm) and from 1×10^{-15}–5×10^{-15} m^2 down to 6×10^{-18}–2×10^{-20} m^2 for the small initial apertures ($b_o = 0.32$–0.61 mm), as shown in Fig. 15. Because the intact claystone matrix is practically impermeable at the applied gas pressures below 1 MPa, the permeability of fractured claystone is determined exclusively by the fracture closure, which may be approximated by the "cubic law" for fluid flow through a set of parallel fractures:

$$K_g = \frac{R}{12s}b^3 = \frac{F}{12}b^3 \tag{8}$$

where b is the average fracture aperture, s is the mean fracture spacing, R is the roughness factor of the fracture surfaces, and $F = R/s$ represents an integrated character of the set of fractures. As the fracture aperture b decreases to zero, K_g tends to zero. Fitting the data yields different F-values of 1×10^{-5} m^{-1} up to 2×10^{-2} m^{-1} due to the different characteristics of the fractures in samples.

5.2. Under impact of water flow

As water enters and flows through fractures in claystone, the clay matrix can take up water and expand into the interstices. The water-induced swelling, weakening and slaking of the claystone lead to sealing of the fractures. Consequently, the hydraulic conductivity of the fractured claystone decreases. Fig. 16 shows the long-term evolution of water permeability obtained on fractured COX samples under low confining stresses of 2–3.5 MPa over more than 3 years. As soon as the water was supplied, the high initial gas permeability of 3×10^{-12} m^2 dropped immediately by five to seven orders of magnitude down to 10^{-17}–10^{-19} m^2, depending on the fracture intensity of each sample. At each load level, the permeability decreased gradually with time. The final permeability values are very low at 3×10^{-20}–7×10^{-21} m^2, being the same order of magnitude as that of the undisturbed clay rock.

The permeability values K_w obtained after stabilization at different effective confining stresses σ_{eff} are summarized in Fig. 17. The effective stress is defined as $\sigma_{eff} = \sigma - p_w/2$, where σ is the total confining stress, p_w is the water upstream pressure, and $p_w/2$ is the mean pore pressure

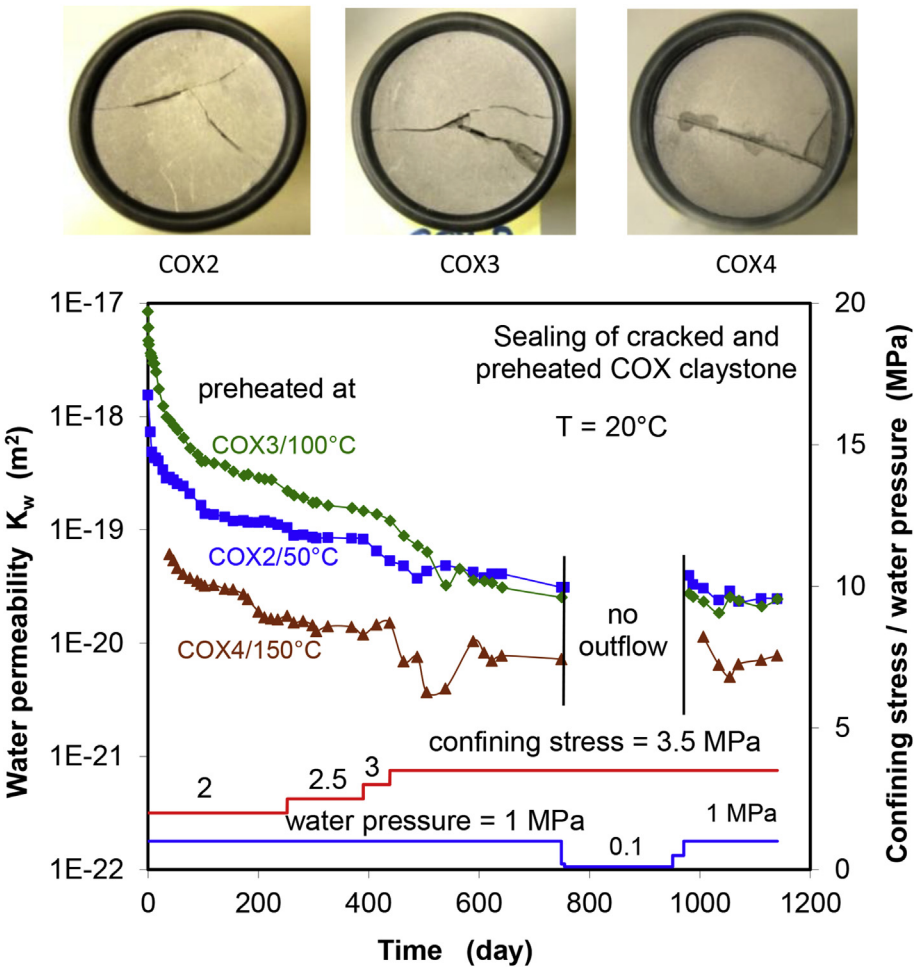

Fig. 16. Long-term evolution of water permeability obtained on fractured COX claystone.

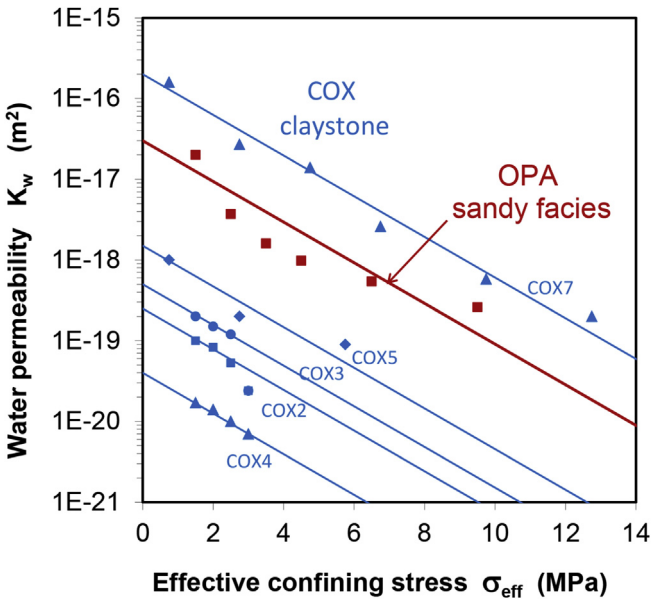

Fig. 17. Water permeability of fractured claystones as a function of confining stress.

at zero downstream pressure. The logK_w-σ_{eff} dataset for each sample can be approximated by an exponential equation:

$$K_w = K_{wo} \exp\left(-\beta \sigma_{eff}\right) \quad (9)$$

where K_{wo} is the water permeability at zero effective stress $\sigma_{eff} = 0$, and β is a parameter characterizing the closure tendency of the pathways. K_{wo} is determined by the initial intensity of fractures in the material and varies from a sample to another, whereas β reflects the effects of swelling and deformation of the claystone matrix near the fracture walls into the fracture voids, and thus can be used as an index for the self-sealing capacity. Different K_{wo}-values are estimated in the range of 2×10^{-16}–4×10^{-20} m^2 and a unique β-value of 0.58 MPa^{-1} is obtained for all tested COX and OPA samples. This is clearly illustrated in Fig. 18 with the normalized permeability to the initial ratio, K_w/K_{wo}. The same slope of the log(K_w/K_{wo})-σ_{eff} curves indicates the same self-sealing capacity of the COX claystone from the −490 m level of the MHM-URL and the OPA sandy claystone from the MT-URL. The OPA sandy claystone has relative lower contents of clay minerals (20%–40%) but higher contents of quartz (30%–45%) and carbonates (20%–40%).

6. Gas migration

Gas generation from corrosion of metallic components and its impact on the integrity of the natural and engineered barrier

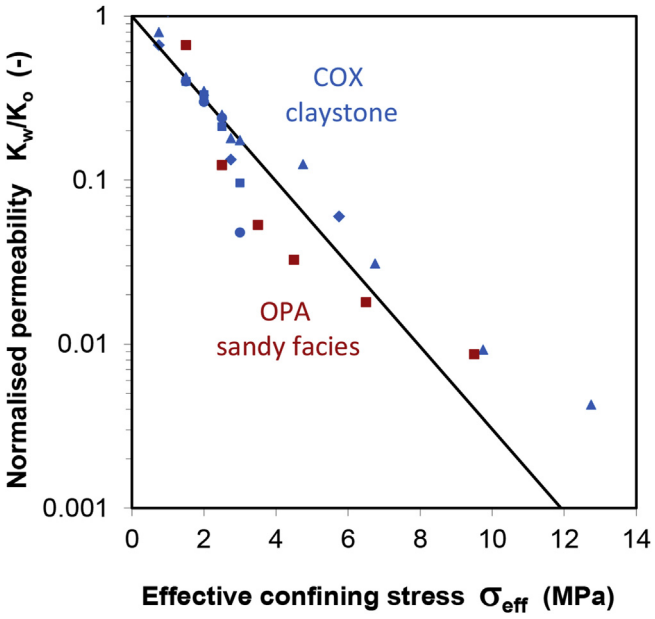

Fig. 18. Normalized permeabilities of the COX claystone and OPA sandy claystone as a function of effective confining stress.

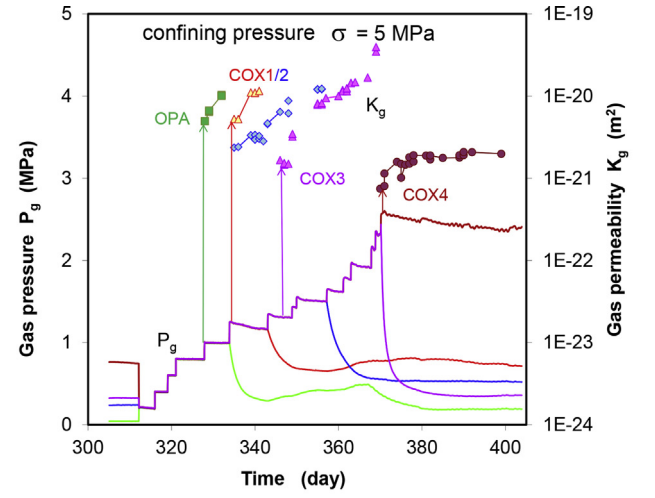

(a)

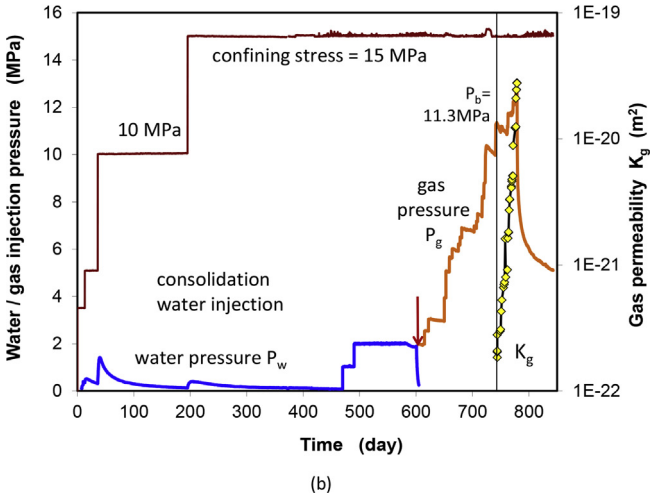

(b)

Fig. 19. Gas breakthrough pressures and permeabilities obtained on highly resealed COX and OPA claystones under different confining stresses: (a) 5 MPa and (b) 15 MPa.

systems is one of the most concerns for the repository safety. This important issue was intensively investigated in the European Commission project – FORGE (Fate Of Repository GasEs) (Shaw, 2015; Zhang, 2015b). The highly-consolidated and water-saturated clay rocks are practically impermeable for advective transport of gas under normally-encountered pressure gradients (Horseman et al., 1996; Rodwell et al., 1999; Cuss et al., 2012; Harrington et al., 2013). However, the EDZ may act as conduits for preferential gas flow, depending on the resealing degree of fractures. The gas migration behavior of damaged claystone was examined on pre-fractured claystone samples that had been fully water-saturated and highly resealed (Zhang, 2015b).

Fig. 19 presents the measured gas breakthrough pressures of the highly resealed samples with very low water permeabilities of 10^{-19}–10^{-21} m^2 (cf. Figs. 16 and 17). It can be seen that gas entry and penetration into the water-saturated and highly resealed claystones need high gas pressures to overcome certain thresholds, which are determined by the sealing intensity of the fractures under confining stress.

The advective gas flow through resealed claystone is accompanied by micro-fissuring and dilation of the generated fissures. Fig. 20 shows an example of the gas pressure impact on a resealed sample under axial stress of 16 MPa and lateral stress of 12.7 MPa. During the first stage with stepwise gas pressure increase from 2 MPa to 4 MPa, compressive strains evolved progressively and no gas outflow was detectable. The subsequent pressure increase to 4.5 MPa inhibited the continuation of the radial compression. Further pressure increase to 5–7 MPa led to a slightly gradual dilatancy in radial direction, indicating a gas penetration into the sample. The pathways are probably attributed to reopening of some weakly resealed fractures under the high gas pressures. As the gas pressure was increased up to 8.3 MPa, a sudden dilatancy in all directions took place and gas breakthrough occurred.

As shown above, the gas breakthrough pressures observed on the highly resealed claystones are still below the minor confining stress and thus below the fracturing criterion for the intact clay rock, as shown in Fig. 21. This important finding implies that the EDZ, even when highly resealed, will still bear the capacity for gas migration with moderate pressures and thus contribute to avoiding high pressure buildup, so that the host rock is prevented from gas fracturing. The gas breakthrough pressure of water-saturated and resealed claystone can

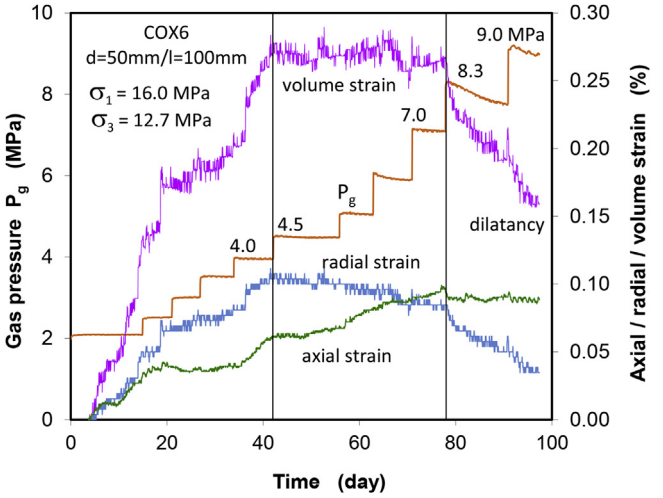

Fig. 20. Gas pressure induced dilatancy in a highly resealed claystone sample under triaxial compression.

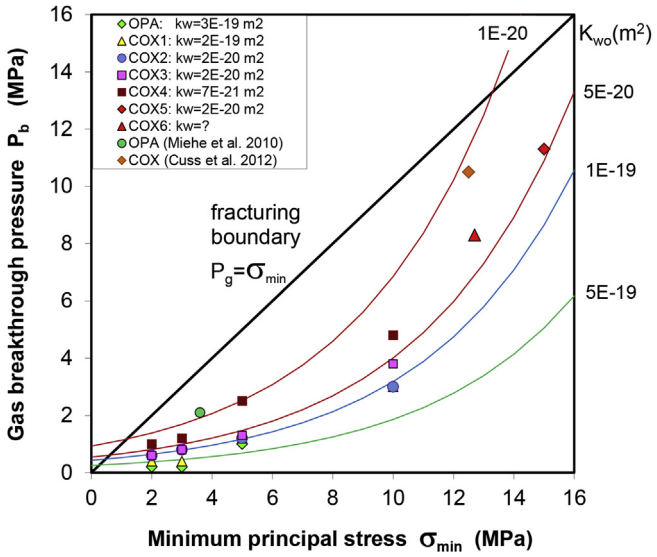

Fig. 21. Gas breakthrough pressures of highly resealed claystones in comparison with a conservative fracturing criterion for intact clay rock.

be expressed as a function of water permeability and minimum confining stress:

$$P_b = B(K_{wo})^{-1/n} \exp(\gamma \sigma_{min}) \quad (10)$$

where P_b is the gas breakthrough pressure, K_{wo} is the initial water permeability at zero minor principal stress $\sigma_{min} = 0$, and the parameters are estimated to be $B = 2 \times 10^{-7}$ MPa m$^{2/3}$, $n = 3$ and $\gamma = 0.2$ MPa^{-1}. The model prediction provides a reasonable agreement with the data as shown in Fig. 21.

Further gas pressure rising can reopen more resealed micro-fissures as well as dilate the gas-occupied pathways. The growth of the micro-fissure networks allows gas to flow easier, so that the gas permeability increases as shown in Fig. 22. The relationship of gas permeability to gas pressure rise can be approximately represented by an exponential function:

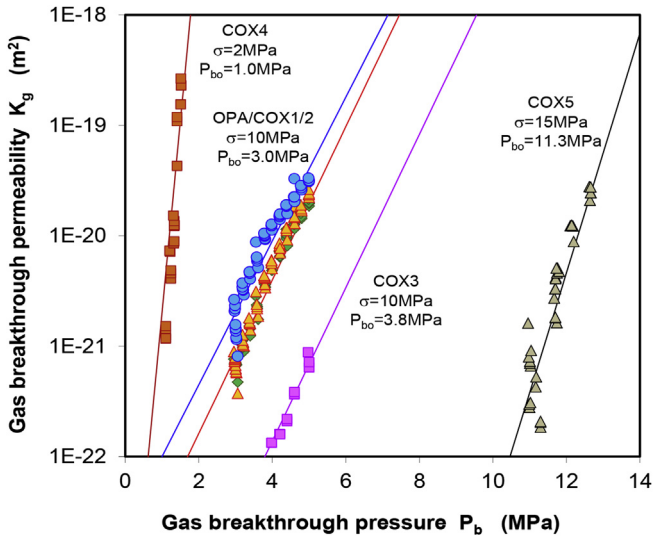

Fig. 22. Gas breakthrough permeability of resealed claystones as a function of gas pressure.

$$K_g = K_{go} \exp[\omega(P_b - P_{bo})] \quad (11)$$

where K_{go} is the gas permeability at the initial breakthrough pressure P_{bo}; and ω is a parameter characterizing the dilatability and interconnectivity of the gas pathways, which can be determined by the slope of the $\ln K_g$-P_b curve. Fitting the data obtained by increasing gas pressure leads to ω-values in a small range of 1.5–2.5 MPa^{-1}.

7. Thermal effects

The most concern over the disposal of heat-emitting HLW is whether and how the favorable barrier properties of the clay host rock will be altered under transient non-isothermal conditions over several thousands of years. This important issue was extensively investigated in the European Commission project – TIMODAZ (Thermal Impact on the Damaged Zone around a Radioactive Waste Disposal in Clay Host Rocks) (Li, 2013). Within this project and the other German national projects, thermal effects on claystones were comprehensively investigated on COX and OPA samples under various repository-relevant conditions (Zhang et al., 2005, 2006; 2007, 2008; 2009, 2010a; 2013; Zhang, 2016b). Thermal effects were measured by hydro-mechanical responses of the claystones to thermal loading, including thermally-induced expansion and contraction, pore pressure variation, temperature influences on deformability and strength, on swelling as well as on self-sealing capacities.

7.1. Thermal expansion

Thermal expansion was measured by heating the claystones with the natural water contents under decreased confining stresses of 15 MPa, 10 MPa, 5 MPa and 1 MPa (Zhang et al., 2013, 2017). Fig. 23 shows the results of a heating test on COX sample at a confining stress of 5 MPa. The water-saturated sample was heated by stepwise increasing temperature from 23 °C to 68 °C and then cooled down. The measured strains (Fig. 23a) show that (1) each temperature increase generates expansion in all directions; (2) the expansion does not change much with time at constant temperatures below 47 °C and then turns over to a gradual contraction at higher temperatures; and (3) cooling down yields contraction. The contraction at the high temperatures above 56 °C might be caused by mobilization of the heated pore water into some unsaturated pores and also by possible leakage of the isolating boundary against such high temperatures, which allows some release of pore water and thus leading to consolidation under loading.

Based on the data, thermal expansion coefficient can be obtained as a function of temperature (Fig. 23b). The coefficient increases almost linearly with increasing temperature in the test range, which can be expressed by

$$\alpha_m = [3\alpha_s(1-\phi) + \alpha_w\phi] + \omega(T - T_o) \quad (12)$$

where α_s, α_w and α_m are the linear expansion coefficient of the solid grains, the volumetric expansion coefficients of the pore water and the water-saturated porous medium, respectively; T and T_o are the actual and the reference temperatures (20 °C), respectively; and ω is a factor. The first term of the right side of the equation represents the thermal expansion coefficient of the material at T_o and the second term for the temperature dependence. The parameter values are obtained by fitting the data for the claystone with a porosity of $\phi = 16.5\%$: $\alpha_s = 2 \times 10^{-6}$ °C^{-1} for clay minerals, $\alpha_w = 3.4 \times 10^{-4}$ °C^{-1} for pore water, $\omega = 1 \times 10^{-6}$ °C^{-1}. Because of the bedding structure, the thermal expansion is anisotropic. The

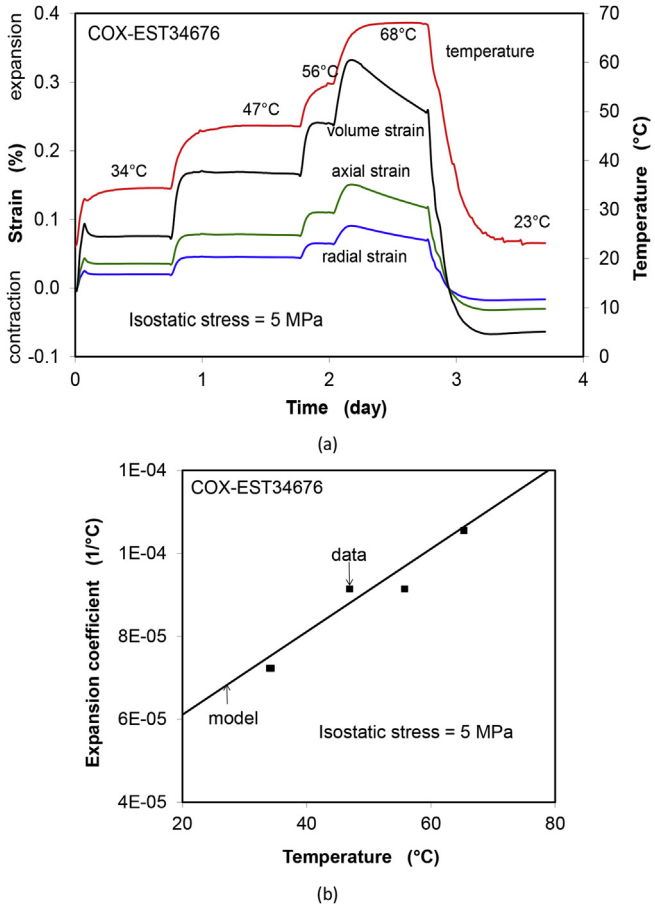

Fig. 23. Thermal expansion and contraction of a COX sample during heating and cooling: (a) Strain response to thermal loading, and (b) Thermal expansion coefficient.

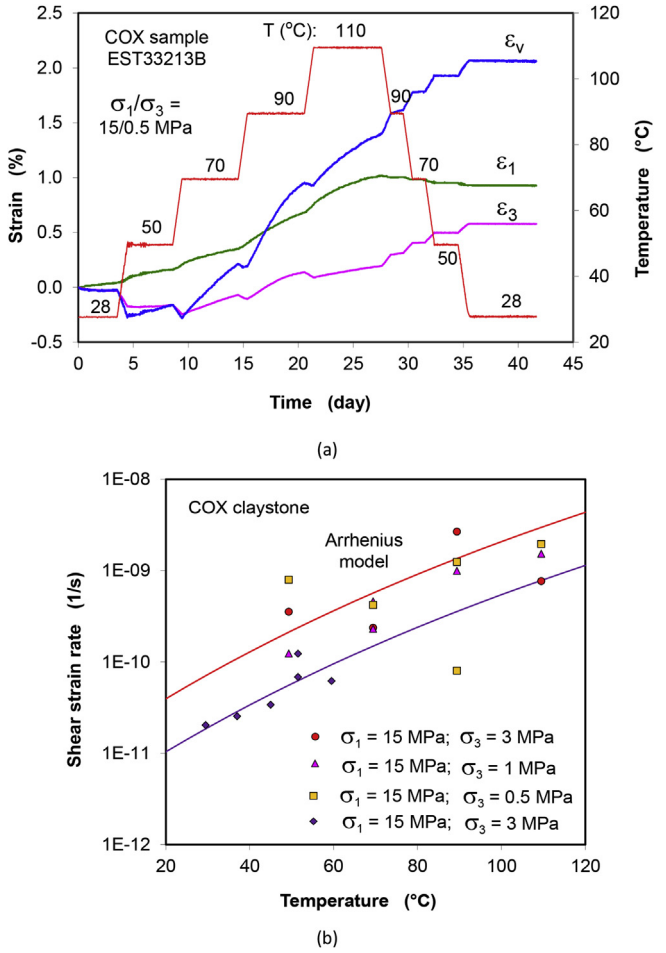

Fig. 24. Temperature influence on the creep of water-saturated COX claystone: (a) Triaxial creep at different temperatures, and (b) Stationary creep rate as a function of temperature.

thermal expansion in direction perpendicular to bedding is higher than that parallel to bedding (Zhang et al., 2008, 2010a; 2013; Zhang, 2016b).

7.2. Temperature influences on deformation and strength

Thermal impact on the deformation of the claystones was examined in triaxial creep tests under various temperatures and stresses. Fig. 24a shows a typical creep test on the water-saturated COX claystone at different temperatures of 28 °C–110 °C under a triaxial stress state of $\sigma_1/\sigma_3 = 15$ MPa/0.5 MPa and undrained conditions. The strain-time curves show that: (a) each temperature increase leads to a short-time radial expansion but a slight axial compression; (b) the axial, radial and volumetric strains (ε_1, ε_3, ε_v) increases quite linearly with time at each elevated temperature below 90 °C, suggesting no or less thermal transient creep; (c) at higher temperatures above 90 °C, the creep slows down; and (d) cooling down results in a short-term radial contraction and negligible creep at each lowered temperature. The creep acceleration at elevated temperatures up to 90 °C probably results from the reduction of viscosity and friction of bound water-films between solid particles. At the higher temperatures, the undrained conditions of the testing system could not be tightly maintained, so that some thermally-mobilized pore water was released up to 2% observed after testing. As a consequence, the pore structure was consolidated, increasing the friction resistance between particles and hence decelerating the creep. Fig. 24b illustrates the steady state creep rate as a function of temperature under different stress conditions. The creep acceleration by temperature up to about 90 °C can be reasonably revealed by the creep equation (Eq. (5)).

Thermal impact on the strength of a claystone differs from saturated to unsaturated states and from drained to undrained conditions. In saturated and undrained conditions, the claystone becomes more ductile and weaker with increasing temperature, as shown in Fig. 25 depicting the undrained stress–strain behavior of the water-saturated OPA claystone at temperatures between 20 °C and 116 °C and at lateral stresses around 3 MPa. The weakness is probably caused by thermally-induced pore overpressure and the corresponding decrease in effective mean stress on one hand and by thermally-induced reduction of the cohesion and friction resistance of the bound water-films between solid particles on the other hand.

However, the temperature influence on the strength of the water-saturated COX claystone is less significant, as shown in Fig. 26 comparing the undrained strength values at $T = 20$ °C–30 °C (black points) and at $T = 40$ °C–100 °C (collar points). The strength curves at different temperatures are close to each other. In contrast to the undrained thermal loading, heating a claystone in drained condition drives the existing water out of the pores, resulting in consolidation of the pore structure under confining stresses, increasing the inner friction resistance between solid particles against shearing and hence strengthening the rock. For instance, heating and drying the COX claystone at high temperatures of 90 °C–

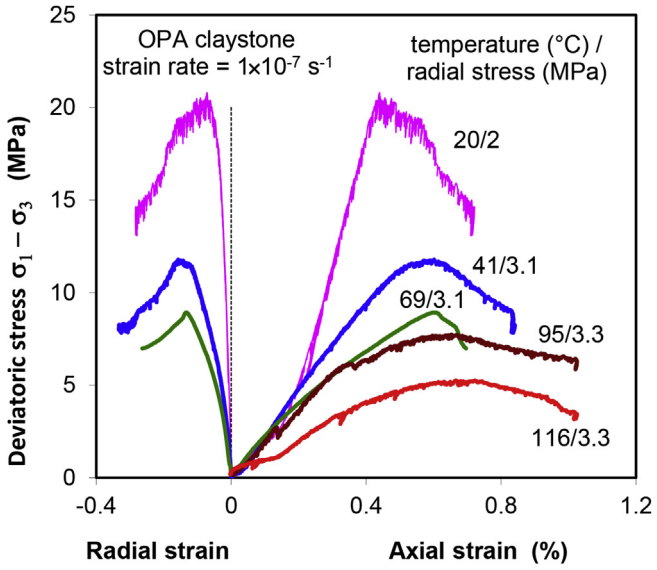

Fig. 25. Stress–strain curves obtained on the water-saturated OPA claystone at different temperatures.

150 °C (upper part in Fig. 26) can increase the strength of the claystone significantly.

7.3. Thermal impact on self-sealing of fractures

Thermal impact on the self-sealing capacity of damaged claystone is one of the most concerns in the assessment of the long-term safety of HLW repositories. This was examined by measuring water permeability of fractured claystones in various thermal conditions. Fig. 27a shows the evolution of water permeability obtained on cracked COX and OPA samples during heating and cooling between 20 °C and 90 °C. As soon as the water was supplied, the high initial gas permeability of 3×10^{-12} m^2 dropped immediately by two to five orders of magnitude down to 10^{-15}–10^{-17} m^2, depending on the fracture intensity of each sample. This drastic drop in permeability is mainly attributed to the water-induced swelling, slaking and clogging of the fractures. During the first stage at 20 °C, the water permeability decreased with time from 1×10^{-15} m^2 to 3×10^{-18} m^2 at OPA sample and from 1×10^{-17} m^2 to 5×10^{-19} m^2 at COX sample, respectively. The permeability reduction rate was less affected by the temperature increase up to 60 °C. Further heating up to 90 °C and also cooling down back to 60 °C had no or only little effect on the permeability reached before. Further cooling down to 20 °C, however, induced a further reduction of the permeability to 3×10^{-19} m^2 and 1×10^{-19} m^2 at both the samples.

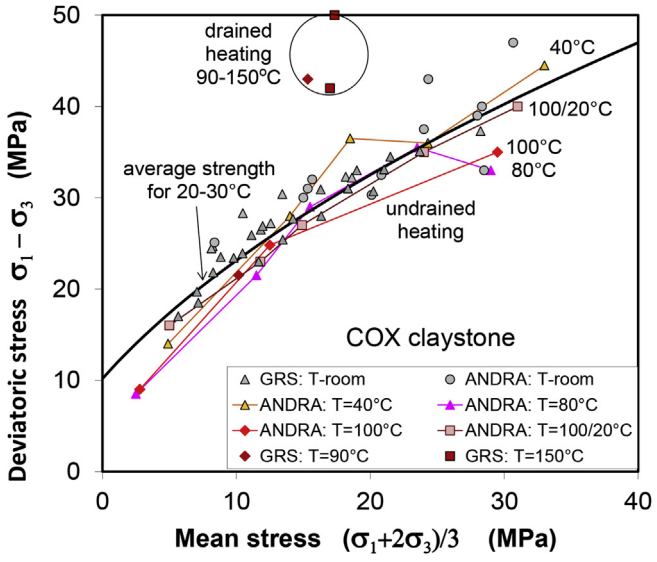

Fig. 26. Comparison of drained and undrained thermal strengths of the COX claystone.

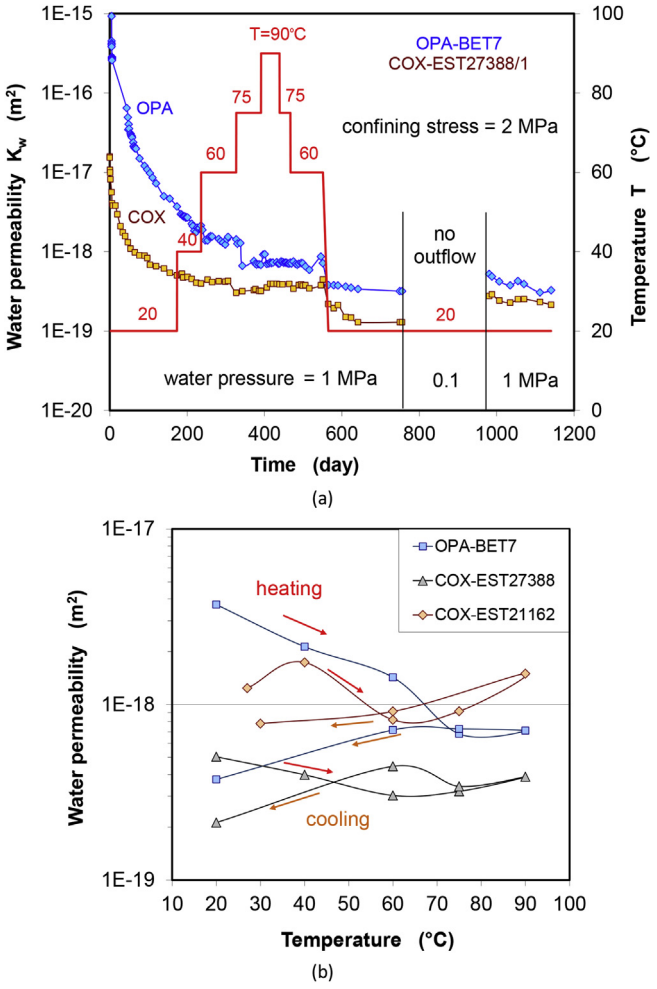

Fig. 27. Temperature influence on the water permeability of fractured COX and OPA claystones: (a) Water permeability evolution during heating/cooling, and (b) Water permeability as a function of temperature.

The water permeability values obtained after stabilization of each temperature stage are depicted in Fig. 27b as a function of temperature. It is obvious that the permeabilities of the fractured claystones are slightly influenced by heating and cooling. They decrease more or less with increasing temperature during heating and drop further down with cooling. Generally speaking, the self-sealing capacity of fractures in the claystones is not remarkably affected by the applied thermal load.

8. Conclusions

The THM behavior of the COX and OPA clay rocks has been extensively investigated with various kinds of laboratory experiments, covering the important aspects concerning the long-term containment of radioactive waste: (1) stress concept, (2) deformability and damage, (3) moisture effects, (4) self-sealing of fractures, (5) gas migration, and (6) thermal impacts.

The stress analysis suggests that the interparticle or effective stress in a dense clay-water system is transferred through both the adsorbed interparticle pore water in narrow pores and the solid-solid contact between non-clay mineral grains. The experiments confirm that the adsorbed pore water in the claystones is capable of bearing effective stresses until the strength is exceeded.

The claystones deform elasto-plastically under rapid load with an overall volume compaction until the onset of dilatancy at a high stress. Closely as the peak stress is reached, shear fractures are created leading to a spontaneous increase in permeability and to failure. The damage and failure are suppressed under high values of the minor confining stress. After failure, the claystone still possesses a certain residual strength. When the minor principal stress is increased again, the fractures tend to be closed. The long-term deformability of the claystones is characterized by creep under constant load. The creep under relatively low shear stresses is probably dominated by diffusion and slip processes in the bound water-films between solid particles. At high stresses above the dilatancy threshold, the creep is enhanced by microcracking through the interfaces between particles and tends towards rupture.

The claystones are sensitive to moisture change. In dry air conditions or high suctions, the pore water moves out of the pore space, leading to shrinkage or compaction of the desaturated pores under load. It enhances the friction resistance between particles and hence the stiffness and strength. In contrast, the claystones can take up water from a humid environment, resulting in expansion or development of swelling pressure under confinement. The enlargement of distances between particles due to water uptake leads to degradation of the stiffness and strength.

The claystones possess significant self-sealing potentials. Fractures in them are going to close up under mechanical compression. The fracture aperture decreases exponentially with the increasing normal confining stress. The resulting decrease in gas permeability is related to the aperture by a cubic law. As water enters and flows through fractures, the clay matrix takes up water and expands into the interstices. Consequently, the hydraulic conductivity decreases dramatically by several orders of magnitude down to low levels of 10^{-19}–10^{-21} m^2 even at low confining stresses of 2–4 MPa. The decreased water permeabilities are in the same order of the intact claystones.

Before water saturation, fractures in the claystones act as preferential pathways for gas. After water saturation, gas entry and subsequent penetration into the resealed fractures require a certain gas pressure to overcome the breakthrough threshold, which is controlled by the re-sealing degree of fractures and the confining stress. All the experiments show that the gas breakthrough pressures in the water-saturated and highly resealed claystones are still lower than the confining stresses. It implies that the EDZ, even when highly resealed, will still have the capacity for gas migration at moderate pressures.

Thermal impacts on the properties and responses of the claystones are dependent on their inherent properties such as porosity and water saturation, and also on the external conditions such as confining stress, hydraulic drained and undrained boundaries. In the water-saturated claystones, the thermal expansion is predominantly controlled by the pore water because of its much higher expansion coefficient compared to that of the solid grains. Under undrained and confined conditions, the water expansion causes high pore pressures, thus the effective stress decreases. The thermal mobilization of the bound pore water alters the inherent cohesion and friction resistance between particles, accelerating the deformation but decreasing the strength. In contrast, heating in drained conditions drives the thermally mobilized pore water out of the pore space. Under external load, the release of the bound pore water leads to consolidation of the porous medium. With heating and drying, the contacts between particles become increasingly the solid-to-solid type, so that the friction resistance between particles increases, enhancing the stiffness and strength but hindering the creep. Another key point is that the high sealing potentials of the fractured claystones are almost not affected by the applied thermal loads at 90 °C–120 °C, so that the favorable barrier properties of the clay host rocks will not be altered during the thermal loading from HLW.

Conflict of interest

The author wishes to confirm that there are no known conflicts of interest associated with this publication and there has been no significant financial support for this work that could have influenced its outcome.

Acknowledgements

This work was funded by the German Federal Ministry for Economic Affairs and Energy (BMWi) under contract number 02E10377.

References

Amann F, Wild KM, Loew S, Yong S, Thoeny P, Fran E. Geomechanical behaviour of Opalinus clay at multiple scales: results from Mont Terri rock laboratory (Switzerland). Swiss Journal of Geosciences 2017;110(1):151–71.

Andra. Sthesis – eynvaluation of the feasibility of a geological repository in an argillaceous formation. DOSSIER 2005 Argile report. Andra. 2005.

Andra. Status of the cigéo project in France - French industrial geological disposal project. In: Proceedings of the LUCOEX conference and workshop, Oskarshamn, Sweden; 2015.

Armand G, Bumbieler F, Conil N, de la Vaissière R, Bosgiraud JM, Vu MN. Main outcomes from in situ thermo-hydro-mechanical experiments programme to demonstrate feasibility of radioactive high-level waste disposal in the Callovo-Oxfordian claystone. Journal of Rock Mechanics and Geotechnical Engineering 2017;9(3):415–27.

Auvray C, Grgic D, Morlot C, Fourreau E, Talandier J. X-ray tomography applied to self-sealing experiments on argillites. In: Proceedings of the 13th international congress of international society for rock mechanics (ISRM). Innovations in applied and theoretical rock mechanics. ISRM; 2015.

Bernier F, Lemy F, De Cannière K, Detilleux V. Implications of safety requirements for the treatment of THMC processes in geological disposal systems for radioactive waste. Journal of Rock Mechanics and Geotechnical Engineering 2017;9(3):428–34.

Blümling P, Bernier F, Lebon P, Martin CD. The excavation damaged zone in clay formations: time-dependent behaviour and influence on performance assessment. Physics and Chemistry of the Earth 2007;32(8–14):588–99.

Bock H, Dehandschutter B, Martin CD, Mazurek M, Haller AD, Skoczylas F, Davy C. Self-sealing of fractures in argillaceous formations in the context of geological disposal of radioactive waste – review and synthesis. Clay Club Report No. 6184. NEA; 2010.

Bossart P, Jaeggi D, Nussbaum C. Experiments on thermo-hydro-mechanical behaviour of opalinus clay at Mont Terri rock laboratory, Switzerland. Journal of Rock Mechanics and Geotechnical Engineering 2017;9(3):502–10.

Chen WZ, Ma YS, Yu HD, Li FF, Li XL, Sillen X. Effects of temperature and thermally-induced microstructure change on hydraulic conductivity of Boom Clay. Journal of Rock Mechanics and Geotechnical Engineering 2017;9(3):383–95.

Conil N, Talandier J, Djizanne H, de La Vaissière R, Righini-Waz C, Auvray C, Morlot C, Armand C. How rock samples can be representative of in-situ condition: a case study of Callovo-Oxfordian claystones. Journal of Rock Mechanics and Geotechnical Engineering 2018;10(4). https://doi.org/10.1016/j.jrmge.2018.02.004.

Cuss RJ, Harrington JF, Giot R, Auray C. Experimental observations of mechanical dilation at the onset of gas flow in callovo-oxfordian claystone. In: Proceedings of the 5th international meeting – clay in natural and engineered barriers for radioactive waste confinement; 2012.

Davy CA, Skoczylas F, Barnichon FD, Lebon P. Permeability of macro-cracked argillite under confinement: gas and water testing. Physics and Chemistry of the Earth 2007;32(8–14):667–80.

Harrington JF, Cuss RJ, Noy DJ. Dilatancy driven gas flow in the callovo-oxfordian claystone. In: FORGE international symposium and workshop – gas generation and migration; 2013.

Horseman ST, Higgo JJW, Alexander J, Harrington JF. Water, gas and solute movement through argillaceous media. Nuclear energy Agency report CC-96/1. Paris: OECD; 1996.

Jobmann M, Bebioka A, Burlaka V, Herold P, Jahn S, Lommerzheim A, Maßmann J, Meleshyn A, Mrugalla S, Reinhold K, Rübel A, Stark L, Ziefle G. Safety assessment methodology for a German high-level waste repository in clay formations. Journal of Rock Mechanics and Geotechnical Engineering 2017;9(5):856–76.

Li XL. TIMODAZ: a successful international cooperation project to investigate the thermal impact on the EDZ around a radioactive waste disposal in clay host rocks. Journal of Rock Mechanics and Geotechnical Engineering 2013;5(3):231–42.
Marschall P, Giger S, De La Vassiere R, Shao H, Leung H, Nussbaum C, Trick T, Lanyon B, Senger R, Lisjak A, Alcolea A. Hydro-mechanical evolution of the EDZ as transport path for radionuclides and gas: insights from the Mont Terri rock laboratory (Switzerland). Swiss Journal of Geosciences 2017;110(1):173–94.
Mazurek M, Gautschi A, Marschall P, Vigneron G, Lebon P, Delay J. Transferability of geoscientific information from various sources (study sites, underground rock laboratories, natural analogues) to support safety cases for radioactive waste repositories in argillaceous formations. Physics and Chemistry of the Earth 2008;33:95–105.
Menaceur H, Delage P, Tang AM, Conil N. The thermo-mechanical behavior of the Callovo-Oxfordian claystone. International Journal of Rock Mechanics and Mining Sciences 2015;78:290–303.
Menaceur H, Delage P, Tang AM, Conil N. On the thermo-hydro-mechanical behaviour of a sheared Callovo-Oxfordian claystone sample with respect to the EDZ behaviour. Rock Mechanics and Rock Engineering 2016a;49(5):1875–88.
Menaceur H, Delage P, Tang AM, Talandier J. The status of water in swelling shales: an insight from the water retention properties of the Callovo-Oxfordian claystone. Rock Mechanics and Rock Engineering 2016b;49(12):4571–86.
Minardi A, Crisci E, Ferrari A, Laloui L. The role of anisotropy on the volumetric behaviour of Opalinus Clay upon suction change. In: Ferrari A, Laloui L, editors. Advances in laboratory testing and modelling of soils and shales (ATMSS), Springer series in geomechanics and geoengineering. Springer; 2017. https://doi.org/10.1007/978-3-319-52773-4_36.
Mitchell JK. Characteristics and mechanisms of clay creep and creep rupture. In: Clay-water interface and its rheological implications. Clay Mineral Society; 1992. p. 212–44.
Mitchell JK. Fundamentals of soil behavior. Berkeley, USA: University of California; 1976.
Nagra. Project Opalinus clay, models, codes and data for safety assessment – demonstration of disposal feasibility for spent fuel, vitrified high-level waste and long-lived intermediate-level waste. Technical report. 2002. p. 02–6.
Nagra. Beurteilung der geologischen Unterlagen für die provisorischen Sicherheitsanalysen in SGT Etappe 2. Klärung der Notwendigkeit ergänzender geologischer Untersuchungen. Technical report NTB 10-01. Wettingen, Switzerland: Nagra; 2010 (in German).
Nagra SGT. Etappe 2: vorschlag weiter zu untersuchender geologischer Standortgebiete mit zugehörigen Standortarealen für die Oberflächenanlage. Geologische Grundlagen. Technical report NTB 14-02. Wettingen, Switzerland: Nagra; 2014 (in German).
NEA Clay Club. Clay characterization from nonoscopic to microscopic resolution. In: Workshop proceedings, Karlsruhe, Germany; 2011.
Noynaert L. Heat and radiation effects on the near field of a HLW or spent fuel repository in a clay formation (CERBERUS Project). EUR 19125EN, Contract No. F14W-CT95–0008. 2000.
Robinet JC, Sardini P, Siitari-Kauppi M, Prêt D, Yven B. Upscaling the porosity of the Callovo-Oxfordian mudstone from the pore scale to the formation scale; insights from the 3H-PMMA autoradiography technique and SEM BSE imaging. Sedimentary Geology 2015;321:1–10.
Rodwell WR, Harris AW, Horseman ST, Lalieux P, Müller W, Ortiz Amaya L, Pruess K. Gas migration and two-phase flow through engineered and geological barriers for a deep repository for radioactive waste. A Joint EC/NEA Status Report, European Commission, EUR 19122 EN. 1999.
Rutter EH. Pressure solution in nature, theory and experiment. Journal of Geological Society 1983;140:725–40.
Shaw RP. Gas generation and migration in deep geological radioactive waste repositories. Geological society special publication No. 415. London: The Geological Society of London; 2015.
Tsang CF, Barnichon JD, Birkholzer J, Li XL, Liu HH, Sillen X. Coupled thermo-hydro-mechanical processes in the near field of a high-level radioactive waste repository in clay formations. International Journal of Rock Mechanics and Mining Sciences 2012;49:31–44.
Valès F, Nguyen Minh D, Gharbi H, Rejeb A. Experimental study of the influence of the degree of saturation on physical and mechanical properties in Tournemire shale (France). Applied Clay Science 2004;26(1):197–207.
Wan M, Delage P, Tang AM, Talandier J. Water retention properties of the Callovo-Oxfordian claystone. International Journal of Rock Mechanics and Mining Sciences 2013;64:96–104.
Wang L, Bornert M, Chanchole S. Micro-scale experimental investigation of deformation and damage of argillaceous rocks under hydric and mechanical loads. In: Poromechanics V; 2013. p. 1635–43.
Yang D, Chanchole S, Valli P, Chen L. Study of the anisotropic properties of argillite under moisture and mechanical loads. Rock Mechanics and Rock Engineering 2013;46:247–57.
Yu L, Weetjens E, Sillen X, Vietor T, Li XL, Delage P, Labiouse V, Charlier R. Consequences of the thermal transient on the evolution of the damaged zone around a repository for heat-emitting high-level radioactive waste in a clay formation: a performance assessment perspective. Rock Mechanics and Rock Engineering 2014;47:3–19.
Yven B, Sammartino S, Geroud Y, Homand F, Villieras F. Mineralogy texture and porosity of Callovo-Oxfordian claystones of the Meuse/Haute-Marne region (eastern Paris Basin). Mémoires de la Société géologique de France 2007;178:73–90.
Zhang CL, Wileveau Y, Rothfuchs T. A heating experiment in the Opalinus clay at the Mont Terri rock laboratory. In: Proceedings of the 10th international conference on environmental remediation and radioactive waste management; 2005.
Zhang CL, Rothfuchs T, Wieczorek K, Jockwer N, Wileveau Y. Monitoring and modeling of responses of the Opalinus Clay to heating. Chinese Journal of Rock Mechanics and Engineering 2006;25(4):659–69 (in Chinese).
Zhang CL, Rothfuchs T, Su K, Hoteit N. Experimental study of the thermo-hydro-mechanical behaviour of indurated clays. Physics and Chemistry of the Earth 2007;32(8–14):957–65.
Zhang CL, Rothfuchs T, Su K. Laboratory experiments on the thermal effects on clay rocks. In: Proceedings of the 3rd international conference on coupled THMC processes in geo-systems, GEOPRO2008; 2008.
Zhang CL, Wieczorek K, Rothfuchs T, Armand G, Lebon P. Responses of the Opalinus clay to heating during the HE-d experiment at Mont Terri. In: Proceedings of the european commission TIMODAZ-THERESA international conference; 2009. p. 397–401.
Zhang CL, Czaikowski O, Rothfuchs T. Thermo-hydro-mechanical behaviour of the Callovo-Oxfordian clay rock. Final report of the BURE-HAUPT/EC-TIMODAZ project, GRS-266. 2010.
Zhang CL, Wieczorek K, Xie ML. Swelling experiments on mudstones. Journal of Rock Mechanics and Geotechnical Engineering 2010b;2(1):41–7.
Zhang CL, Czaikowski O, Rothfuchs T, Wieczorek K. Thermo-hydro-mechanical processes in the nearfield around a HLW repository in argillaceous formations – volume I: laboratory Investigations. Project report GRS-312. 2013.
Zhang F, Hu DW, Xie SY, Shao JF. Influences of temperature and water content on mechanical property of argillite. European Journal of Environmental and Civil Engineering 2014;18(2):173–89.
Zhang CL, Conil N, Armand G. Thermal effects on clay rocks for deep disposal of high-level radioactive waste. Journal of Rock Mechanics and Geotechnical Engineering 2017;9(3):463–78.
Zhang CL, Rothfuchs T. Experimental study of hydro-mechanical behaviour of the Callovo-Oxfordian argillites. Applied Clay Science 2004;26(1):325–36.
Zhang CL, Rothfuchs T. Moisture effects on argillaceous rocks. In: Schanz T, editor. Proceedings of the 2nd international conference on mechanics of unsaturated soils. Springer; 2007. p. 319–26.
Zhang CL, Rothfuchs T. Damage and sealing of clay rocks detected by measurements of gas permeability. Physics and Chemistry of the Earth 2008;33(Supp. 1):363–73.
Zhang CL. Self-sealing of fractures in argillites under repository conditions. In: International conference and workshop in the framework of the EC TIMODAZ and THERESA projects; 2009.
Zhang CL. Experimental evidence for self-sealing of fractures in claystone. Physics and Chemistry of the Earth 2011;36(17–18):1972–80.
Zhang CL. Sealing of fractures in claystone. Journal of Rock Mechanics and Geotechnical Engineering 2013;5(3):214–20.
Zhang CL. Deformation of clay rock under THM conditions. Geomechanics and Tunnelling 2015a;8(5):426–35.
Zhang CL. Investigation of gas migration in damaged and resealed claystone. In: Shaw RP, editor. Gas generation and migration in deep geological radioactive waste repositories. Geological society special Publication No. 415. London: The Geological Society of London; 2015b.
Zhang CL. The stress-strain-permeability behavior of clay rock during damage and recompaction. Journal of Rock Mechanics and Geotechnical Engineering 2016a;8(1):16–26.
Zhang CL. Experimental study of thermal effects on clay rock for deep disposal of radioactive waste. In: Proceedings of the 1st international conference on energy geotechnics, ICEGT 2016; 2016.
Zhang CL. Examination of effective stress in clay rock. Journal of Rock Mechanics and Geotechnical Engineering 2017a;9(3):479–89.
Zhang CL. Response of clay rock to moisture change. In: Proceedings of the international workshop ATMSS 2017 – Advances in laboratory testing and modelling of soils and shales, Springer series in geomechanics and geoengineering. Springer; 2017b. p. 155–64.

Chun-Liang Zhang obtained his BSc and MSc degrees in Mining Engineering from Liaoning Technical University, China, in 1982 and 1984, respectively, and his PhD in Mining Engineering from Technical University of Clausthal, Germany, in 1990. He was affiliated as scientific staff with German National Research Center for Environment and Health (GSF) from 1990 to 1993, German Federal Institute for Geosciences and Natural Resources (BGR) from 1993 to 1998, Underground Research Laboratory Asse Mine from 1998 to 2001, and Repository Safety Research Division of the Gesellschaft fuer Anlagen-und Reaktorsicherheit (GRS) - Germany's leading expert organization in the nuclear safety field, since 2001. His research interests include (1) experimental investigations on the thermo-hydro-mechanical (THM) behaviors of host rocks (clay, salt) and engineered barrier materials (clay-based mineral mixtures, crushed salt, etc.) for deep geological disposal of nuclear waste; and (2) theoretical study and numerical modeling of coupled THM processes in the natural-engineered barrier systems in repositories. He has been participated in a number of European and German national projects.